# 11 Current Clinical Imaging of Hypoxia with PET and Future Perspectives

Mareike Roscher, Carmen Wängler, Stefan O. Schönberg, and Björn Wängler

## Contents


11.1 **Introduction** ..... 242

11.2 **PET Tracers Used in Hypoxia Imaging** ..... 244
11.2.1 [$^{18}$F]Fluorodeoxyglucose ..... 245
11.2.2 Nitroimidazole-Based PET Radiotracers ..... 246
11.2.3 Cu-Diacetyl-bis(N$^4$-methylthiosemicarbazone) (Cu-ATSM) ..... 258
11.2.4 Anti-Carbonic Anhydrase IX (CAIX) Antibodies ..... 260

11.3 **Integrin-Specific PET Tracers: An Indirect Marker for Tumor Hypoxia?** ..... 262

11.4 **Treatment Planning in Therapy After Hypoxia PET Imaging** ..... 262

**Conclusion** ..... 263

**References** ..... 263



M. Roscher • B. Wängler (✉)
Institute of Clinical Radiology and Nuclear Medicine, Medical Faculty Mannheim of Heidelberg University, Molecular Imaging and Radiochemistry, Theodor-Kutzer-Ufer 1-3, 68167 Mannheim, Germany
e-mail: mareike.roscher@medma.uni-heidelberg.de; bjoern.waengler@medma.uni-heidelberg.de

C. Wängler
Institute of Clinical Radiology and Nuclear Medicine, Medical Faculty Mannheim of Heidelberg University, Biomedical Chemistry, Theodor-Kutzer-Ufer 1-3, 68167 Mannheim, Germany
e-mail: carmen.waengler@medma.uni-heidelberg.de

S.O. Schönberg
Institute of Clinical Radiology and Nuclear Medicine, University Medical Center Mannheim, Medical Faculty Mannheim of Heidelberg University, Theodor-Kutzer-Ufer 1-3, 68167 Mannheim, Germany
e-mail: stefan.schoenberg@umm.de


## Abbreviations

| | |
|---|---|
| ACRIN | American College of Radiology Imaging Network |
| ATSM | Diacetyl-bis(N$^4$-methylthiosemicarbazone) |
| BOLD | Blood oxygen level dependent |
| CAIX | Carbonic anhydrase IX |
| CT | Computed tomography |
| DAHANCA | Danish Head and Neck Cancer Group |
| EF5 | 2-(2-nitro-1H-imidazol-1-yl)-*N*-(2,2,3,3,3-[$^{18}$F]pentafluoropropyl)-acetamide |
| EPR | Electron paramagnetic resonance |
| FAZA | Fluoroazomycin arabinoside |
| FDG | Fluorodeoxyglucose |
| FETA | Fluoroetanidazole |
| FETNIM | Fluoroerythronitroimidazole |
| FMISO | Fluoromisonidazole |
| GLUT-1 | Glucose transporter-1 |
| IAZA | Iodoazomycinarabinoside |
| GTV | Gross tumor volume |
| HIF-1 | Hypoxia-inducible transcription factor-1 |
| HNC | Head and neck cancer |
| IMRT | Intensity-modulated radiation therapy |

A. Luna et al. (eds.), *Functional Imaging in Oncology*,
DOI 10.1007/978-3-642-40412-2_11, © Springer-Verlag Berlin Heidelberg 2014

| | |
|---|---|
| MISO | Misonidazole |
| MRI | Magnetic resonance imaging |
| NSCLC | Non-small cell lung cancer |
| PET | Positron Emission Tomography |
| p.i. | Post injection |
| PTSM | Pyruvaldehyde-bis ($N^4$-methyl thiosemicarbazone) |

## 11.1 Introduction

Hypoxia is a characteristical pathophysiological property of most tumors and occurs as a consequence of inadequate blood supply [1]. If tumors reach a diameter of a few millimeters, for instance, in locally advanced lesions or in rapidly growing tumors, the oxygen supply generally stays persistently behind the requirements of the tumor despite neovascularization [2]. This reflects the structural and functional disorganization of tumor vasculature resulting in disturbed microcirculation (acute hypoxia) and intercapillary distances that are beyond the diffusion range of oxygen (chronic hypoxia) [3, 4]. Thus, the classification of chronic and acute hypoxia is of limited validity [5] as the blood flow as well as the capacity of hemoglobin to deliver oxygen to cells may vary resulting in changing partial pressures for $O_2$. Additionally, also the nutrients and the pH can change in hypoxic tissues [3]. Hypoxic areas are distributed heterogeneously within a given tumor population regarding incidence and severity [4, 6]. Tumor hypoxia could be shown to be an adverse prognostic and predictive factor in several different entities like cervical cancer, soft tissue sarcoma, and head and neck cancer [5, 7] as it leads to alterations in the (patho) physiome of cells.

Biochemists define hypoxia as $O_2$-limited electron transport [8], whereas clinicians define it as a state of reduced $O_2$ availability or decreased $O_2$ partial pressure restricting or even abolishing functions of organs, tissues, and cells [9, 10]. The use of the term hypoxia in this context describes the clinical definition of hypoxia reflecting the imbalance between cellular $O_2$ consumption rate and $O_2$ supply to the cells [5, 6].

Since the beginning of the twentieth century, the role of hypoxia in tumor resistance is known as molecular oxygen could be shown to be a critical determinant of the response of cells to radiation [11, 12]. Oxygen plays a pivotal role in radiation therapy, a process known as oxygen enhancement effect. "Normal," oxygenated tissues display an oxygen partial pressure of about 45–50 mmHg (5 mmHg correspond to ~0.7 % $O_2$ in the gas phase or 7 μM in solution). If the $O_2$ partial pressure is reduced to values less than 25–30 mmHg, the sensitivity of cells is progressively limited. Oxygen is a potent radiosensitizer resulting from its high electron affinity. After absorbing the energy from ionizing radiation, free radicals are formed leading to DNA damage or modifications in other biologic molecules within the cells. Under hypoxic conditions, up to three times higher doses are required to achieve the same cytotoxic effects as under normoxic conditions [13, 14]. Additionally, many chemotherapies are oxygen dependent as they lead to the generation of free oxygen radicals such as doxorubicin and bleomycin. On top, the biologic alterations resulting from hypoxia as the effects on cell cycle or alterations in proteome hamper the success of chemotherapeutic treatments (as reviewed in [5]). In addition and due to the disturbed microcirculation or the increased expression of multidrug resistance transporters (e.g., P-glycoprotein), the exposure of cells to chemotherapeutics might be reduced [15, 16].

Thus, hypoxia can either result in impaired growth and cell death or act as a factor leading to malignant progression and increased therapy resistance [7, 17–19]. In the latter case, hypoxia is a strong selection pressure for cells inducing a vicious circle of hypoxia and subsequent malignant progression [6]. Hereby, it compromises many biological functions [1], for example, the cell cycle progression arresting the cells in $G_1$/S phase or lengthening the $G_1$ phase disproportionately [20–22], promoting genomic instability and thereby increasing the mutation rate [6, 23]. Furthermore, gene expression and proteomic profiles are changed with an increase in transcription and translation of survival and growth factors, angiogenic molecules, chaperones, and proteins involved in tumor invasiveness facilitating metastasis of the tumor and leading to a more

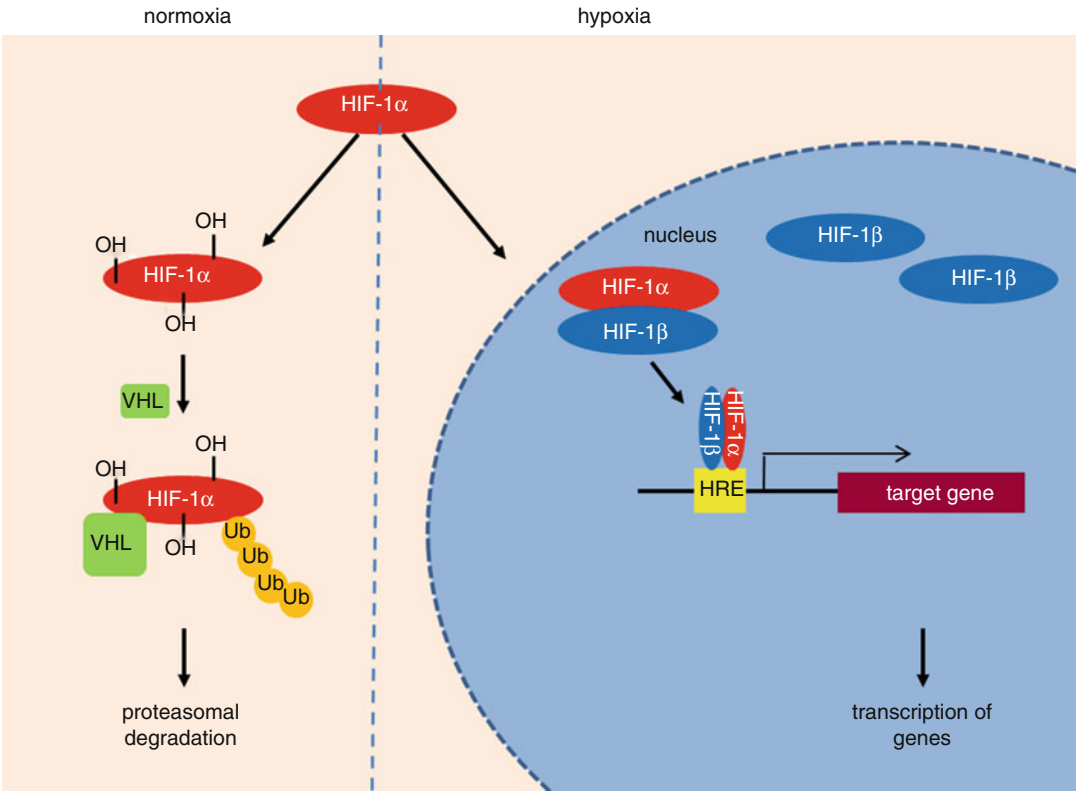


**Fig. 11.1** Schematic pathways of hypoxia-inducible factor-1 (HIF-1). HIF-1α is under normoxic conditions enzymatically hydroxylated enabling the tumor suppressor von Hippel-Lindau (VHL) to bind. This leads to the ubiquitination and proteasomal degradation of HIF-1α. If the cell, however, turns hypoxic, HIF-1α is no longer hydroxylated. VHL cannot interact with the HIF-1α increasing the half-life of the molecule. HIF-1α can enter the nucleus and as heterodimer with HIF-1β bind to hypoxia-responsive element (HRE) domains on the DNA resulting in the transcription of more than 100 target genes involved among others in angiogenesis, glucose metabolism, metastasis, and pro-survival pathways

malignant phenotype resistant to cell death and altered metabolism [24, 25]. For instance, the higher expression of the glucose transporter-1 (GLUT-1) that can be a result of hypoxia correlates with a poorer outcome in breast cancer, head and neck cancer (HNC), and non-small cell lung cancer (NSCLC) [26–28], while carbonic anhydrase IX (CAIX) is implicated to play a role in tumor cell survival and invasiveness [29, 30]. The best characterized molecule which alters the signaling pathways during hypoxia is the hypoxia-inducible transcription factor-1 (HIF-1) (Fig. 11.1). This heterodimer consisting of HIF-1α and HIF-1β binds in its reduced state to hypoxia responsive elements on the DNA increasing the transcription of genes responsible for angiogenesis, erythropoiesis, energy metabolism, and glucose transport into the cell. Consequently, cell survival and oxygen supply is supported [31]. Under normoxic conditions, HIF-1α is rapidly ubiquitinated and degraded with a half-life of about 10 min, whereas it is stabilized under hypoxic conditions [31]. Additionally, also the expression of HIF-1 can be enhanced. High levels of HIF-1α could be shown to be associated with a poorer treatment response and clinical outcome in breast cancer, HNC, as well as in NSCLC and stomach cancer [32–37] making it an attractive candidate for drug targeting [38, 39]. The alterations in hypoxic cells might explain delayed recurrences, dormant micrometastases, and growth retardation in large tumor masses [5].

Studies using oxygen microelectrodes, several different MRI and electron paramagnetic

resonance (EPR) approaches, and detection of exogenous (e.g., misonidazole, 2-(2-nitro-1H-imidazol-1-yl)-N-(2,2,3,3,3-[$^{18}$F] pentafluoropropyl)-acetamide(EF5), or pimonidazole) or endogenous [e.g., HIF-1, CAIX, GLUT-1] molecular markers of cellular hypoxia with immunohistochemical or noninvasive imaging techniques all show that hypoxia is a common feature of tumors in patients presenting for therapy, as well as in animal tumors.

As hypoxia is associated with radiation- and chemoresistance (especially if the tumor areas include tumor-initiating stem cells), it does need not only to be detected in tumors but ideally also to be quantified with the help of predictive biomarkers [4]. Several invasive and noninvasive methods for measuring hypoxia are already established or in development – each with its own advantages and limitations. The question which technique is superior for a clinical or experimental setting depends on the available applications, on the degree of invasiveness, and the resolution required. So far the "gold standard" is intratumoral polarographic measurement of $O_2$ partial pressures which is not appropriate for monitoring the development within the tumor mass during treatment due to its invasiveness. Furthermore, this technique is limited in its application because only random measurements at some sites within a tumor can be performed. Minimally invasive tools such as serum-based diagnostics and global gene signatures are under investigation [4]. Additionally, also the blood oxygen level-dependent (BOLD) effect can be measured via MRI noninvasively as well using paramagnetic deoxyhemoglobin and diamagnetic oxyhemoglobin as an endogenous hypoxia marker (Chap. 12). Hence, this method depends on the perfusion of tumor tissue with red cells, a prerequisite which is not always fulfilled [7]. Next to magnetic resonance imaging (MRI), especially PET imaging has emerged as a promising noninvasive tool to detect and monitor tumor oxygenation. Deeper insights into anatomical and biological information about the tumor might be revealed using PET/CT after applying sensitizer adducts which on top allows to more precisely estimate the location of the hypoxic areas and the quantification of hypoxia levels [40].

## 11.2 PET Tracers Used in Hypoxia Imaging

The imaging of hypoxia with PET has several advantages as the measurements allow a repeated noninvasive whole tumor assessment in vivo. This is one of the major advantages as an estimation of the temporal and spatial distribution of hypoxia can be monitored in the course of a treatment [41]. Nevertheless, hypoxia tracers have to meet several characteristics: they have to be retained specifically in hypoxic cells via an oxygen-specific mechanism with a fast blood clearance to reach appropriate concentrations even in perfusion-limited regions and to generate low concentrations of nonspecific metabolites. Furthermore, hypoxia tracers should allow a repeatable, simple, nontoxic, and fast assessment of local oxygen levels with a high spatial resolution. Another objective in measuring tumor hypoxia via PET is to ensure the reproducibility of the tracer distribution and thresholding irrespective of the operator interpreting the data. The tracers which are currently in use give promising results but do not fulfill all of these requirements [42] which is the reason for the ongoing development of novel tracers with improved imaging properties.

Most of the different hypoxia tracers for PET imaging used so far are bioreductive molecules which will be described in the following sections. Among these, the halogenated PET nitroimidazole agents labeled with F-18 and I-124 have a quite long history, whereas Cu-diacetyl-bis($N^4$-methylthiosemicarbazone) (Cu-ATSM) has only recently been proposed for PET imaging [43].

The major caveat of using PET imaging for hypoxia is that it is usually only a loco- or even microregional effect with patches of cells dispersed throughout the tumor. As the resolution of PET scanners is limited due to the physical characteristics of the used radionuclides and the varying spatial resolutions of 2–4 mm that can

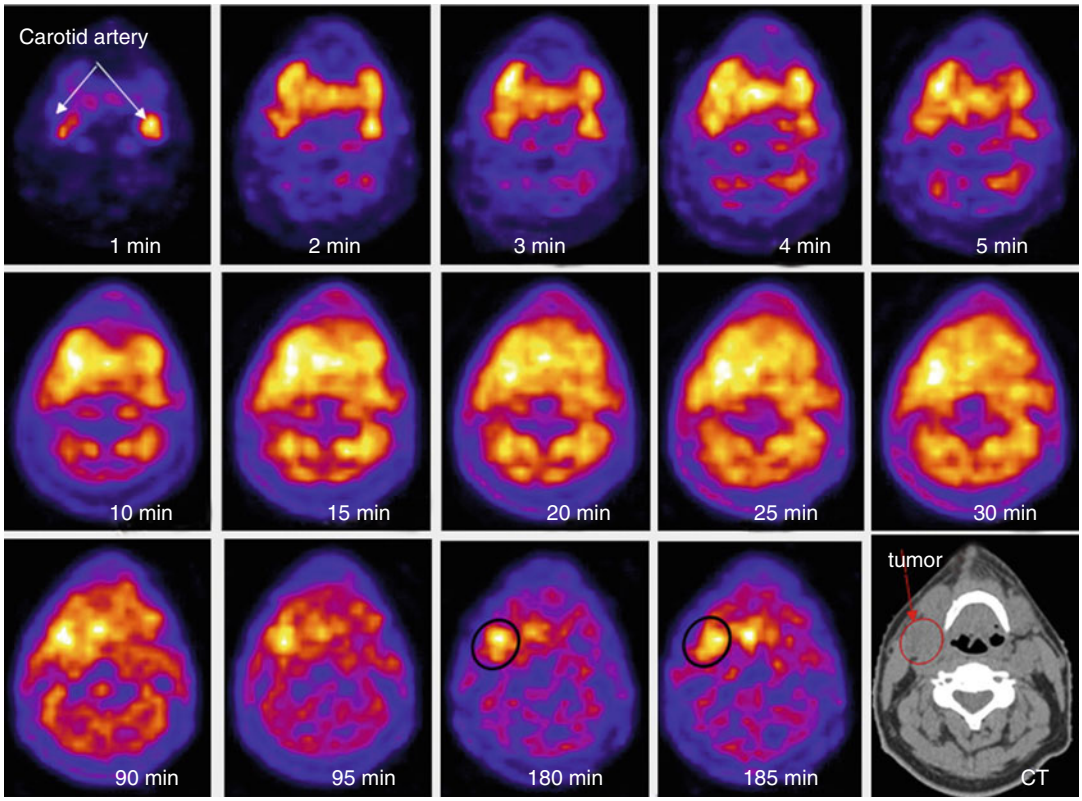


**Fig. 11.2** Optimized characterization of tracer uptake in tumors applying dynamic PET scans. Compared to static PET scans allowing the assessment of standardized uptake values, dynamic scans can provide additional data about the movement and rate of uptake of the applied PET tracer allowing for a more complete diagnosis. After injection of [$^{18}$F]FMISO in a patient with HNC, the dynamic PET scan was applied as a function of time: the first five images taken were of 1 min duration and then 5 frames with 5 min duration followed. The patient was reimaged at 90 min and 180 min after injection. The distribution of [$^{18}$F]FMISO can be tracked from the initial blood pool to the specific accumulation within the tumors. The images were co-registered with low-dose CT scan (*last image*) Reprinted with kind permission of SNMMI from: Carlin and Humm [44])

be achieved by standard clinical scanners, the exact level of hypoxia and its distribution are difficult to locate and quantify so far. In consequence, partial volumes are averaged, giving rise to statistical uncertainties. Hence, the suboptimal signal-to-noise ratio is a concern for the clinical use. These limitations might at least partially be overcome by dynamic imaging employing a kinetic modeling approach (Fig. 11.2). In contrast to single-time-point PET images, dynamic hypoxia PET can distinguish between tumor hypoxia and circulating radiotracer [44]. Dynamic scans, however, are expensive, complex to analyze, and cause inconvenience to patients [45].

### 11.2.1 [$^{18}$F]Fluorodeoxyglucose

[$^{18}$F]Fluorodeoxyglucose ([$^{18}$F]FDG) is the most commonly used PET tracer in clinical routine for oncologic imaging as it allows a sensitive but unspecific detection of many tumors. In hypoxic cells, the mitochondrial ATP synthesis drops; the cells stimulate the Pasteur effect. Furthermore, HIF-1 stimulates the expression of GLUT-1 transporting FDG into the cells [46]. However, the Warburg epigenetic phenotype in normoxic tumor cells leads to a higher uptake of FDG in cells decreasing the possibility to detect hypoxia in malignant tissues. Furthermore, several preclinical and clinical studies could show

that there is no or only a weak correlation between uptake of hypoxia tracers and retention of FDG [47–53]. According to the studies undertaken so far, the use of [$^{18}$F]FDG as biomarker for hypoxia remains questionable. Therefore, a number of hypoxia-specific PET tracers have been developed.

### 11.2.2 Nitroimidazole-Based PET Radiotracers

In the 1970s, nitroimidazoles were discovered as clinical radiosensitizers and first proposed as reducible hypoxia markers in 1979 by Chapman [54, 55]. These molecules mimic the effects of oxygen leading to the sensitization of hypoxic cells to radiation. Nevertheless, if high concentrations of nitroimidazoles were applied which could restore the sensitivity of cells, toxic effects could be observed [56]. For PET imaging very low amounts of the tracers are applied (<15 μg) which do not result in any pharmacologic side effects. One major advantage of nitroimidazoles is that they are less than 5 % protein bound and are therefore distributed efficiently throughout the body even if the blood flow is reduced [57, 58]. On top, they can be applied in immunohistochemistry as well as in PET applications allowing for variable detection techniques of hypoxic tissues, e.g., prior to and after a resection of the tumor.

Nitroimidazoles consist of an imidazole ring with a nitro group at the 2′ position and an additional side chain with different residues at the 1′ position which alters the pharmacokinetic properties of the individual molecules (Fig. 11.3, Table 11.1). In vivo, the $NO_2$ group can be reduced to $NH_2$ if it undergoes a 6-electron intracellular modification: comparable to $O_2$ although with less affinity, the nitro function of nitroimidazoles can accept electrons from the respiratory chain reducing it to the radical anion $–NO_2^-$ (Fig. 11.4). Cellular reductases such as xanthine oxidases with a nitroreductase activity catalyze this reaction and are assumed not to be a limiting factor in this process [59]. In the presence of oxygen, the reactive radical intermediate is reoxidized, as oxygen can accept the electrons from the nitro radical and the parent nitroimidazole can leave the cell via passive diffusion. Under hypoxic conditions, however, the nitroimidazole is further reduced. If a second electron is accepted, the nitroimidazole is irreversibly reduced to an nitroso (–N = O) group. Additional reduction steps lead to the generation of an hydroxylamine (-NHOH)

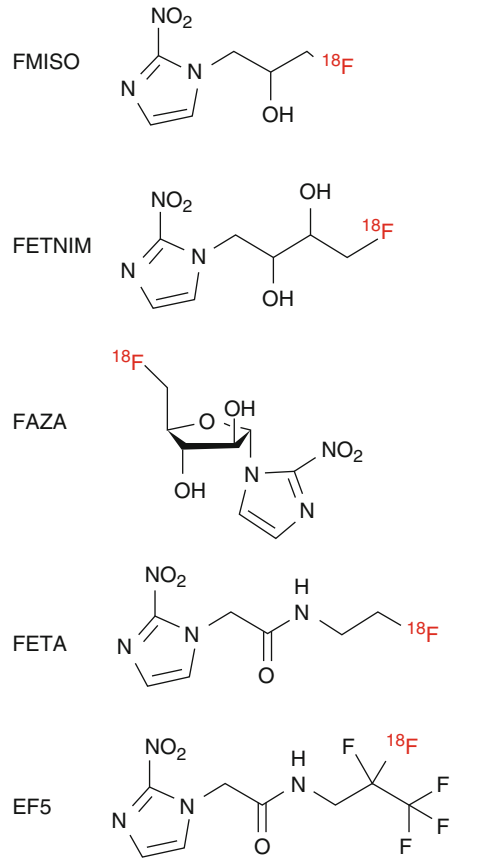


**Fig. 11.3** Structure of nitroimidazole-based PET hypoxia imaging agents

**Table 11.1** Partition coefficients of different nitroimidazoles. The octanol/water partition coefficient depends on the contained alkyl chain

| Nitroimidazole | Alkyl chain | Partition coefficient |
|---|---|---|
| FMISO | $–CH_2CHOCH_2F$ | 0.44 |
| FETNIM | $–CH_2CHOHCHOHCH_2F$ | 0.17 |
| FETA | $–CH_2CONHCH_2CH_2F$ | 0.16 |
| EF5 | $–CH_2CONHCH_2CF_2CF_3$ | 5.7 |

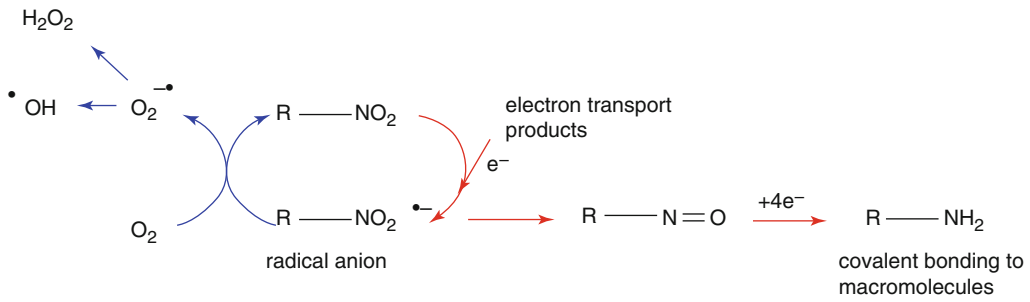


**Fig. 11.4** Mechanism of nitroimidazole retention in hypoxic cells. Nitroimidazoles are reduced by electrons to form radical anions. If oxygen is available, the anion reacts preferentially with this electron acceptor, turning the tracer in its parent state. However, if $O_2$ is not present, the radical anion accepts another electron to produce nitroso- and hydroxylamine intermediates which are sequentially reduced to amines which are cellularly retained. The reactions taking place under normoxic conditions are presented with *blue arrows*, whereas hypoxic reactions are marked with *red arrows*

functionality. This highly reactive hydroxylamine can bind covalently to thiols of macromolecules in the hypoxic cells [38, 60]. Hence, the molecule is entrapped and accumulates within the cells [7, 61, 62]. Due to the dependence of the reactions on electrons from the respiratory chain as well as on the enzymatic activity of nitroreductases, only hypoxic vital cells can be detected. The first observations of nitroimidazole retention within cell spheroids in vitro as well as in tumor models in vivo support this hypothesis [55, 63]. The rate of nitroimidazole accumulation correlates with the degree of hypoxia within the cells allowing for the distinction between normoxia and hypoxia.

To date, several different fluorinated and iodinated nitroimidazole derivates have been developed and tested, a selection of which will be discussed here. As no systematic analysis of all 2-nitroimidazole tracers in the same tumor model or patient group has been undertaken so far, it is difficult to state which tracer is superior to the others in identifying tumor hypoxia.

#### 11.2.2.1 [$^{18}$F]Fluoromisonidazole ([$^{18}$F]FMISO)

[$^{18}$F]Fluoromisonidazole ([$^{18}$F]FMISO) (Fig. 11.3) is the best evaluated and most widely used hypoxia tracer which can be considered as gold standard for PET imaging of hypoxia. The group around Janet Rasey at the University of Washington was the first to propose noninvasive imaging of hypoxia. They pioneered the synthesis of [$^{18}$F]FMISO and demonstrated its feasibility in vivo [57, 64]. The radiosynthesis of [$^{18}$F]FMISO is possible using a commercially available precursor molecule and an automated radiosynthesis protocol. 90–120 min after application, PET measurements result in the best contrast, whereas the early delivery of [$^{18}$F]FMISO depends on the blood flow [42]. The tracer accumulates specifically in hypoxic tissues, and the images obtained unambiguously reflect the regional oxygen partial pressure [61, 65]. The clearance of [$^{18}$F]FMISO from the blood is relatively slow and the tracer distributes via free diffusion in tissues. A reasonable tumor-to-blood cutoff value of $\geq$1.2 is in general used to distinguish normoxia from locoregional hypoxia, and the detection of hypoxia is only possible in viable cells due to the dependency on enzymatic pathways [66]. Even if the blood flow is reduced to one-third, hypoxia and the absence of hypoxia can be detected. The metabolization of [$^{18}$F]FMISO is mainly hepatobiliary but the tracer is also in part excreted via the kidneys resulting in a radiation exposure of patients which is equal or comparable to other radiopharmaceuticals [65, 67, 68].

[$^{18}$F]FMISO can diffuse freely across the blood-brain barrier as it is highly lipophilic and has no protein-binding capacity. As the signal is independent of other factors (altered glucose concentration, pH, and glutathione), [$^{18}$F]FMISO harbors several advantages for imaging [69].

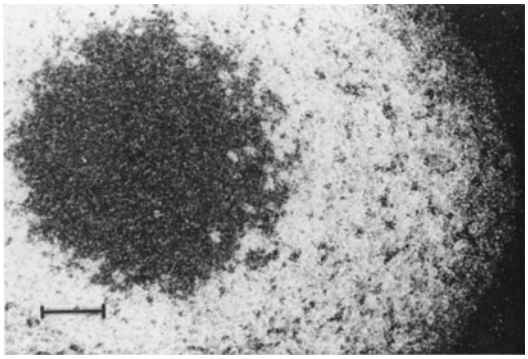

**Fig. 11.5** Uptake of [$^{14}$C]MISO in cellular spheroids. The cell line EMT-6/UW was grown until spheroids of 1 mm were obtained. These were incubated for 8 h with [$^{14}$C]MISO and autoradiographs were taken. The uptake of [$^{14}$C]MISO can be observed in a band of cells surrounding a necrotic core in the center of the spheroid. The normoxic cells in the rim of the spheroid do not accumulate the tracer (The figure was reprinted with kind permission of Radiation Research from Rasey et al. [63])

Furthermore, this nitroimidazole derivative is reduced at any hypoxic site and entrapped within the cells. One major disadvantage of [$^{18}$F]FMISO is the low signal-to-noise ratio resulting in images of limited contrast due to the poor washout [70]. This problem can be overcome by calculating the tumor-to-blood ratio taking a venous blood sample during PET imaging.

The first studies on the uptake of [$^{18}$F]FMISO were performed in vitro with multicellular spheroids. In these aggregates of cells mimicking small tumors, hypoxia could be visualized and quantitatively measured. In Chinese hamster lung V79 spheroids after 4 h of incubation with [$^{3}$H]misonidazole ([$^{3}$H]MISO), and [$^{14}$C] MISO autoradiographs revealed a necrotic center followed by highly tracer-accumulating cells surrounded by the well-oxygenated periphery demonstrating the dependence of tracer entrapment on cell viability (Fig. 11.5) [63]. In monolayer preparations of adult rat myocytes, the relationship between the oxygen concentration and [$^{3}$H]FMISO binding was studied [71]. In comparison to normoxic controls, the [$^{3}$H] FMISO retention after 3 h was about 26 times higher under anoxic conditions; in hypoxic cells the uptake was increased about 15-fold. In a hepatic artery occlusion model in pigs, in vivo

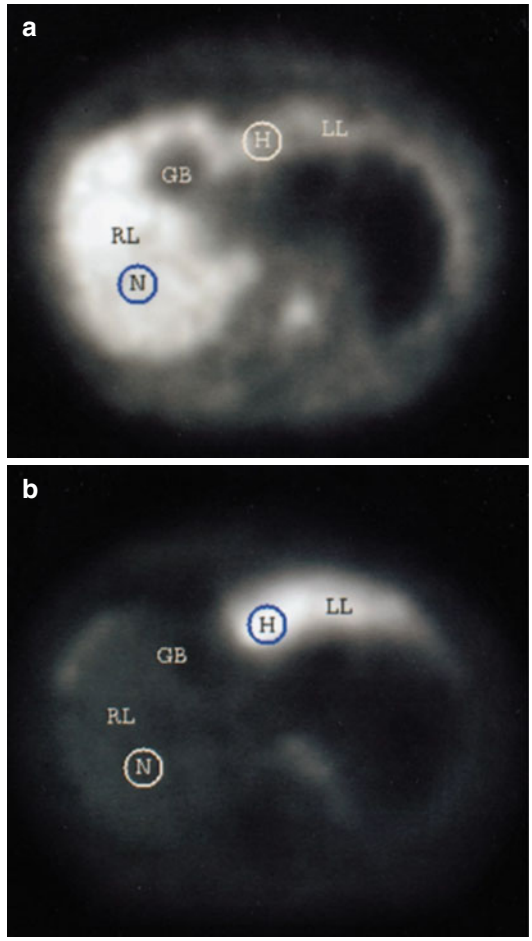


**Fig. 11.6** Detection of hypoxia by [$^{18}$F]FMISO. In domestic pigs liver tissue hypoxia was induced by segmental arterial hepatic occlusion. 3 h after injection of [$^{18}$F]FMISO, dynamic PET scans were performed to measure the specific retention of the tracer within the hypoxic liver segments. This correlated directly to the severity of tissue hypoxia. (**a**) In the first minutes, [$^{18}$F]FMISO displayed high activity in the normally perfused right liver lobe (perfusion), (**b**) while the specific retention in the hypoxic left liver lobe can be observed in later time points (165–180 min). No activity was detected in the gallbladder (*GB*). The circular ROIs indicate normal and hypoxic areas as measured with polarographic electrode measurements before and after PET scanning (The figure was reprinted with kind permission of Springer Science+Business Media from: Piert et al. [72])

hypoxia-dependent [$^{18}$F]FMISO entrapment was shown (Fig. 11.6) [72]. The [$^{18}$F]FMISO accumulation in flow-impaired hepatic segments was about three to four times higher than in normal-flow segments. Polarographic elec-

trode measurements confirmed the correlation between [$^{18}$F]FMSIO uptake and oxygen levels within the tissues.

In vivo, further preclinical studies comparing the results of polarographic measurements and [$^{18}$F]FMISO accumulation have been reported. In a rat tumor model, a good correlation of both parameters could be observed [73], while in C3H mammary cancer xenografts, no correlation was found between the two methods [74]. This might be due to the fact that necrotic tissues with low oxygen levels can be identified as hypoxic using the electrode assessment but do not retain [$^{18}$F] FMISO due to the lack of entrapment of the tracer. A general differentiation between mice with hypoxic and nonhypoxic tumors was possible.

The uptake of [$^{18}$F]FMISO was also analyzed in comparative studies with immunohistochemical staining techniques. The exogenous hypoxia marker pimonidazole and the endogenous hypoxia marker CAIX were compared to [$^{18}$F] FMISO in a rhabdomyosarcoma rat xenograft [75]. The detected hypoxic volumes were significantly correlated underlining the value of [$^{18}$F] FMISO PET to detect hypoxia. Two further studies were undertaken by Troost and colleagues in several xenograft models [76, 77]. They found a correlation between [$^{18}$F]FMISO PET and pimonidazole immunochemistry.

In order to analyze the regional variation in hypoxia within a single tumor which might result from differences in [$^{18}$F]FMISO delivery as well as the oxygen levels in more detail in vivo, studies within one tumor were undertaken [78]. Four hours after injection of [$^{18}$F]FMISO, the freely diffusible blood flow tracer C-14-iodoantipyrine – that has the same partition coefficient as [$^{18}$F] FMISO – was applied to mice. The tumors were dissected into central and peripheral regions, and additional samples were taken from several healthy organs. The tumors generally exhibited a low blood flow, whereas a high blood flow was shown in lungs and kidneys. No correlation between regional flow and [$^{18}$F]FMISO entrapment in individual tumors was found which was also detected for normal tissues. This effect was also observed in larger animals where a very low blood flow was independent of the [$^{18}$F]FMISO retention [58].

Several clinical studies compared the correlation between measurements of partial oxygen pressures and [$^{18}$F]FMISO accumulation as well. In patients with HNC, positive correlations could be found between the two methods [79, 80].

The first study showing the feasibility of [$^{18}$F]FMISO was performed to detect hypoxia in three glioma patients (Fig. 11.7) [81]. Rasey and colleagues could identify hypoxic areas in a variety of tumors prior to treatment [82]. They concluded that human tumor hypoxia is widely prevalent and highly variable inter- and intraindividually.

In clinical studies, it could be shown that the uptake of [$^{18}$F]FMISO correlated with a poor prognosis for patients in HNC and glioblastoma. In patients with HNC 83 % of the tumors have hypoxic subvolumes which were in most cases distributed in single confluent areas, whereas only 22 % were diffusely dispersed [83]. For the patients with HNC, a differentiation between responders and nonresponders to radiotherapy was possible with nonresponders having a higher retention of [$^{18}$F]FMISO although the tumor accumulation varied [49]. A further criterion to differentiate between the two groups was that responders had an initially lower perfusion followed by accumulation of [$^{18}$F] FMISO, whereas the nonresponders showed an initial high perfusion followed by a rapid washout. In glioma patients, the volume and intensity of the detected hypoxia determined prior to radiotherapy showed a strong correlation with a shortened time to progression and overall survival (Fig. 11.8) [84]. For soft tissue tumors, however, [$^{18}$F]FMISO might possibly not be the tracer of choice due to large fractions of necrotic tissue within the tumor lesions [85]. Nevertheless, further studies are required to verify this hypothesis.

In different settings using [$^{18}$F]FMISO, intensity-modulated radiation therapy (IMRT) has been applied and could show next to interindividual differences reproducible results and the feasibility of an imaging-based planning of radiotherapy resulting in a locoregional management of tumors (Fig. 11.9) [86, 87]. Furthermore, in a first study using [$^{18}$F]FMISO PET, the

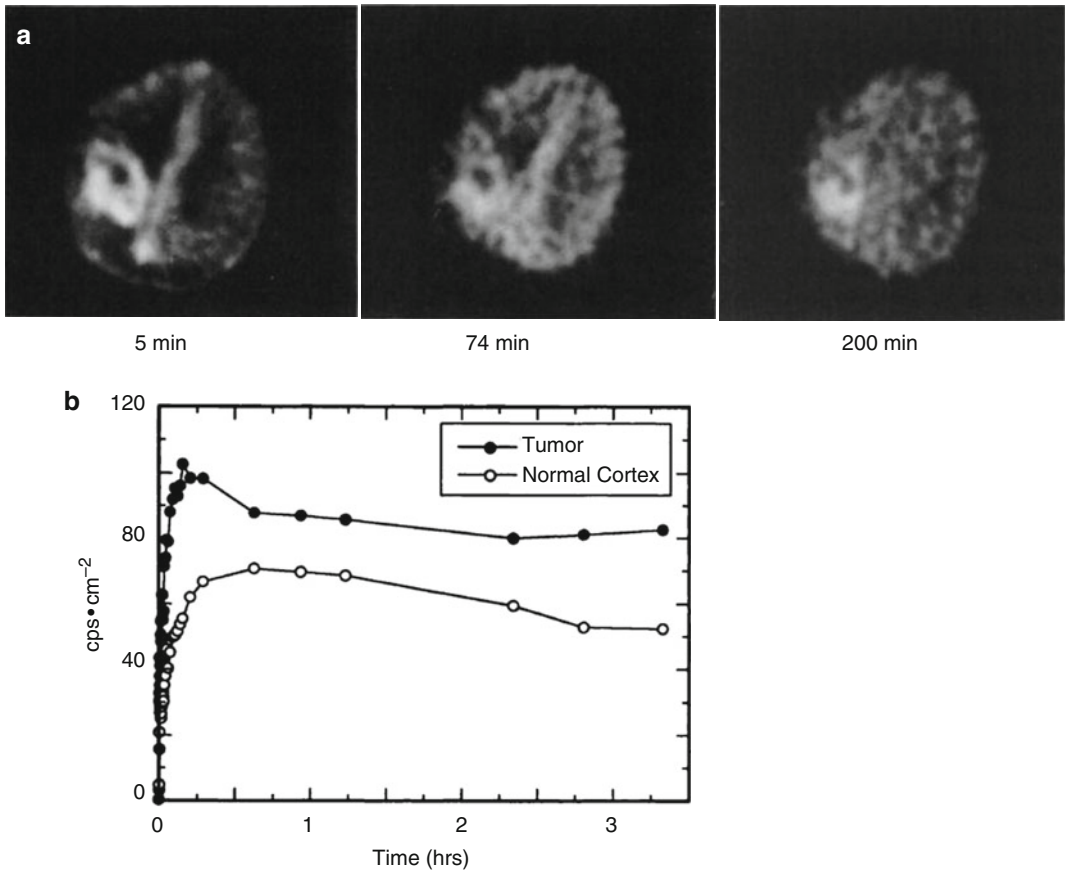


**Fig. 11.7** The first clinical PET scans using [$^{18}$F]FMISO in a patient with malignant glioma. (**a**) 5 min after injecting [$^{18}$F]FMISO, a first tumor activity could be detected. At later time points the uptake in the cortex could be observed although being very slow, indicating a slow passage of tracer across the intact blood-brain barrier. Nevertheless, the activity within the lesion remains higher. (**b**) The time-activity curve for the tumor parallels at about 40 min the curve for the cortical region and the increases to the end of the scanning. These first studies underline the importance of [$^{18}$F]FMISO for PET imaging of hypoxia (Reprinted by permission of SNMMI from: Valk et al. [81])

response to hypoxia-activated chemotherapy using tirapazamine in patients with advanced HNC could be predicted [88].

One preclinical study evaluated the uptake of [$^{18}$F]FAZA and [$^{18}$F]FDG in different cancer cell lines. Whereas [$^{18}$F]FAZA showed an increased retention in hypoxic cells in comparison to normoxic cells, the entrapment of [$^{18}$F]FDG was reduced which could also be shown in tumor xenografts [47]. In clinical studies, similar observations have been reported. In comparison to polarographic measurements, [$^{18}$F]FDG could not differentiate hypoxic from normoxic HNC tissues, whereas [$^{18}$F]FMISO uptake correlated with the partial pressure of oxygen [50, 80]. Further studies compared the retention of [$^{18}$F]FMISO and [$^{18}$F]FDG in patients with HNC, sarcoma, breast cancer, and NSCLC as well as glioma [48–53]. Each of these resulted in no correlation between [$^{18}$F]FDG uptake and hypoxia (Fig. 11.10). Some studies, however, could show a correlation of [$^{18}$F]FDG and [$^{18}$F]FMISO uptake in HNC [52, 89] and brain tumors [90] which calls for further elucidation.

In summary, [$^{18}$F]FMISO has been validated in several different studies for various tumor types. It could be shown to result in variable but significant levels of hypoxia and to be a prognostic indicator with increasing importance [91].

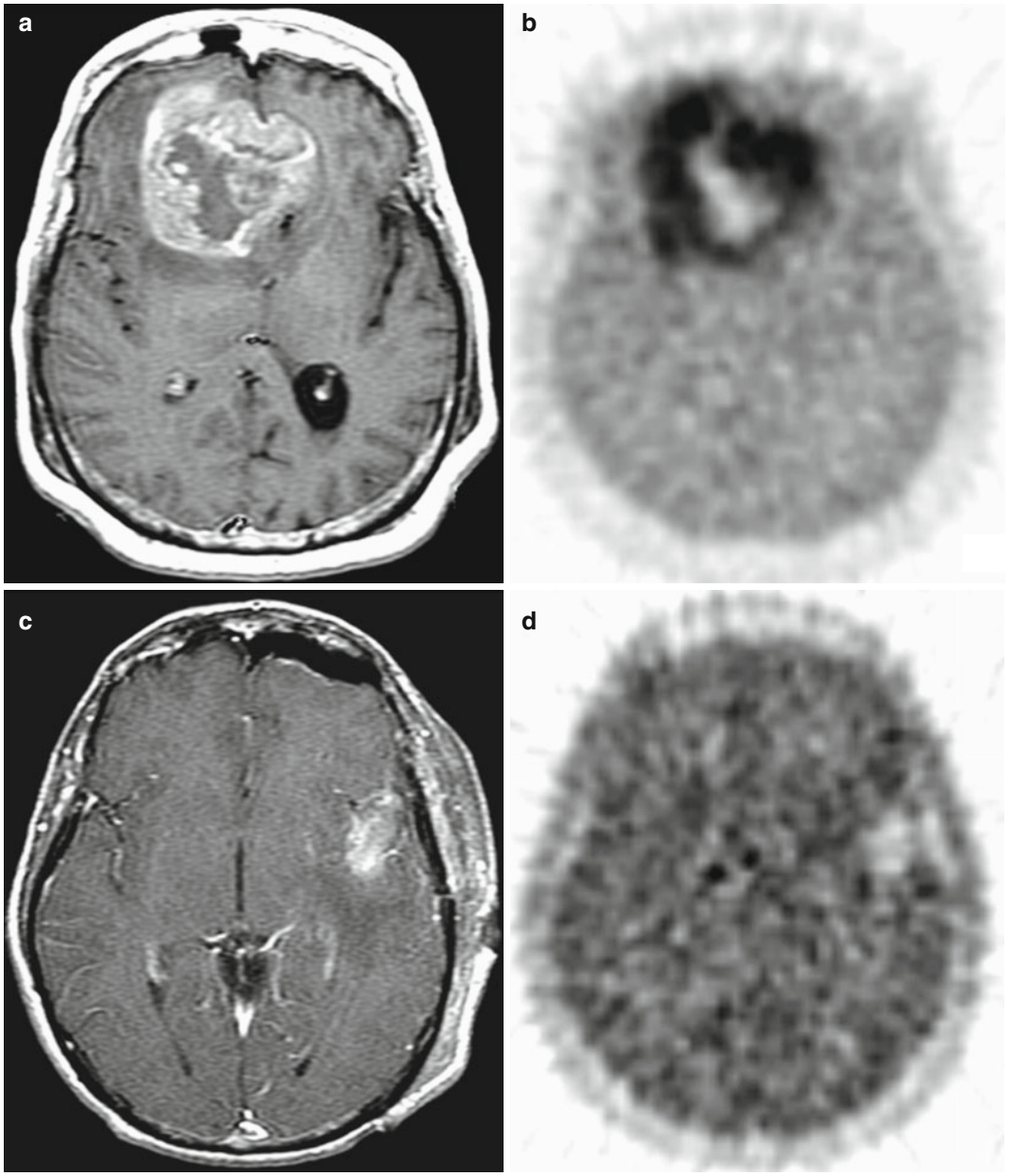


**Fig. 11.8** [$^{18}$F]FMISO accumulation has a predictive value. In patients with glioblastoma multiforme, the [$^{18}$F]FMISO uptake was assessed 2 h p.i. using PET scans before radiotherapy. Tumor-to-blood ratios >1.2 defined the hypoxic value. The burden of hypoxic tissue within the tumor is inversely related to time to tumor progression and survival. (**a**, **c**) The MRI T1Gd images of two patients show the overall tumor size and its localization in the brain. (**b**, **d**) [$^{18}$F]FMISO uptake in the hypoxic areas of the glioma. Especially in patient 1, the high uptake of [$^{18}$F]FMISO can be observed as well as the necrotic center with no retention of the PET tracer (Reprinted with kind permission from AACR from Spence et al. [84])

However, it shows a slow accumulation in hypoxic tumors, a low tumor-to-background ratio, and a significant non-oxygen-dependent metabolism [61].

Next to [$^{18}$F]FMISO several alternative nitroimidazoles have been developed and tested to optimize the pharmaco- and biokinetics in regard to a faster blood clearance, less nonspecific

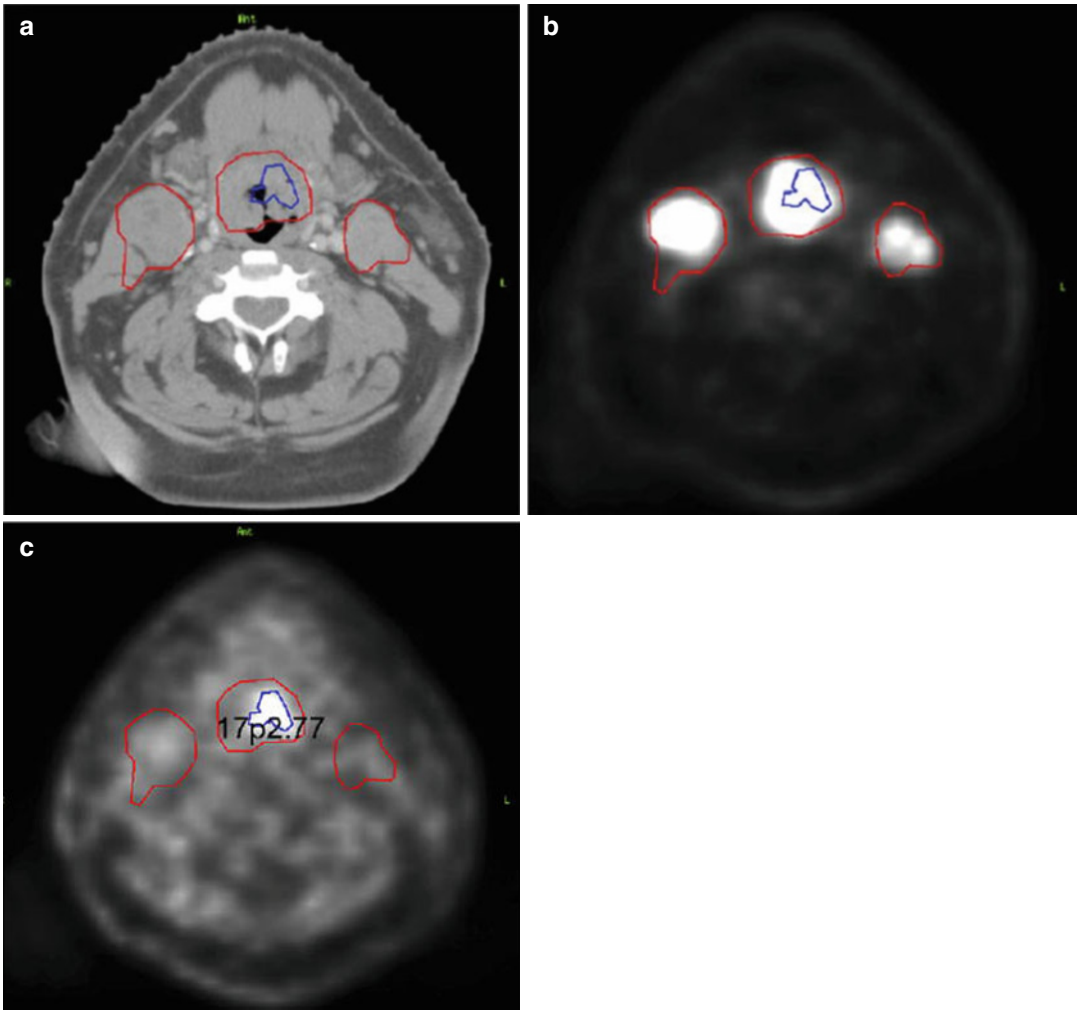


**Fig. 11.9** Feasibility of [$^{18}$F]FMISO PET/CT guided dose-painting IMRT. In HNC patients, the dose escalation to radioresistant hypoxic zones was aimed at while sparing the surrounding normal tissue. The gross tumor volume (GTV) was delineated and the corresponding hypoxic areas determined by [$^{18}$F]FDG PET/CT and [$^{18}$F]FMISO PET/CT image fusion showing (**a**) a CT axial slice, (**b**) an [$^{18}$F]FDG-PET axial scan, and (**c**) an [$^{18}$F]FMISO PET axial slice. This study underlines the importance of multiparametric analyses of tumors for optimizing treatment schemes and to enhance the locoregional control of tumors (Reprinted with permission from Elsevier from Lee et al. [86])

retention, or fewer metabolites of the PET agents. These new agents have to prove to be superior to [$^{18}$F]FMISO in order to gain acceptance [65].

#### 11.2.2.2 [$^{18}$F]Fluoroerythronitroimidazole ([$^{18}$F]FETNIM)

[$^{18}$F]Fluoroerythronitroimidazole ([$^{18}$F]FETNIM) (Fig. 11.3) was first described and evaluated by Yang et al. in 1995 [92]. In mammary tumor-bearing rats, their studies indicated that [$^{18}$F]FETNIM has significantly higher tumor-to-blood and tumor-to-muscle ratios than [$^{18}$F]FMISO at 4 h post injection (p.i.). The pharmacokinetic properties of [$^{18}$F]FETNIM show a low peripheral metabolism and only very little defluorination. The metabolites were hypothesized to be trapped within hypoxic cells [93]. In mice implanted with CH3 mammary carcinomas, [$^{18}$F]FETNIM was investigated in comparison to [$^{18}$F]FMISO under different oxygenation conditions [94]. These studies revealed that [$^{18}$F]FETNIM accumulation correlates with the oxygenation status in the

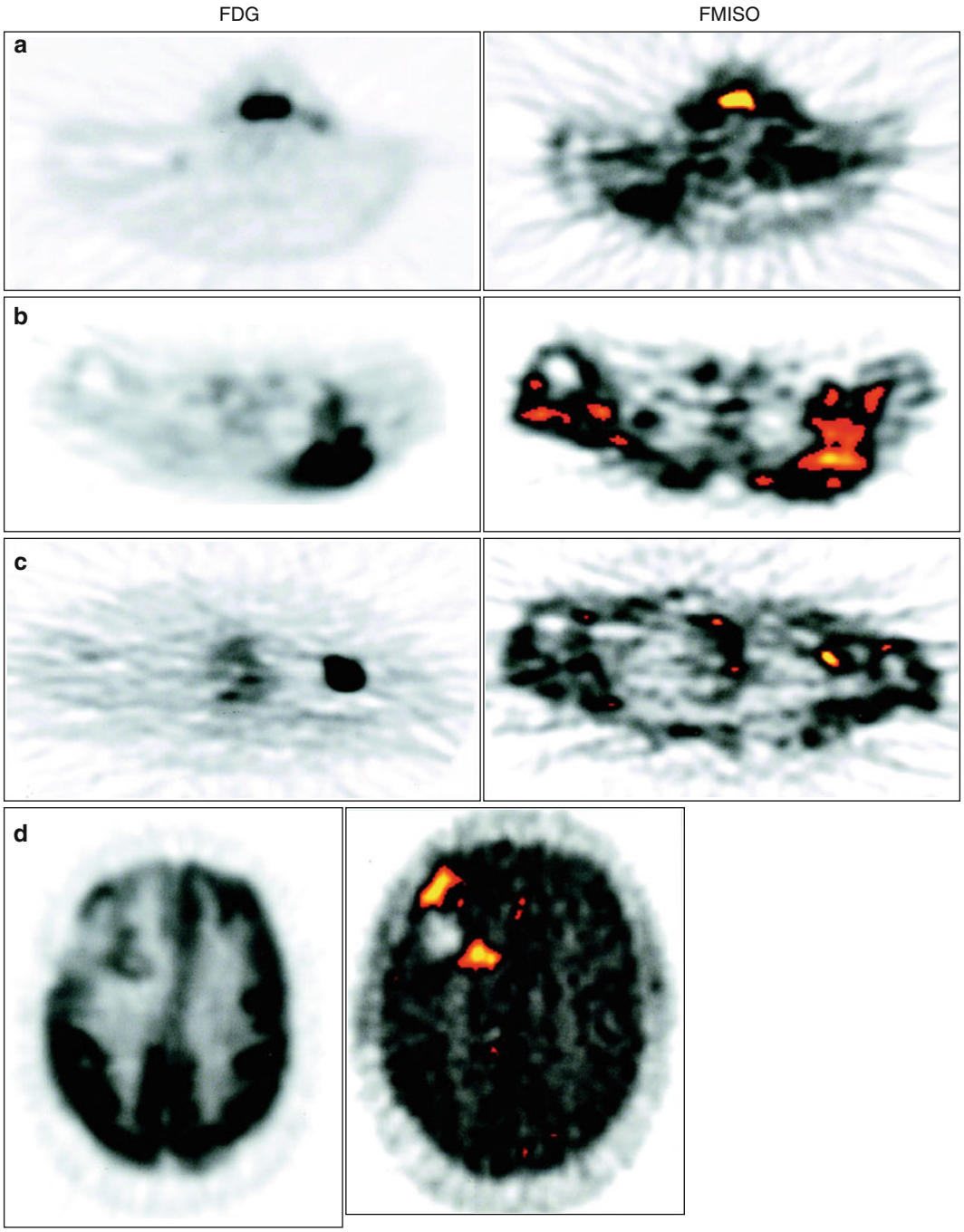


**Fig. 11.10** Relationship between regional hypoxia and glucose metabolism in different tumor entities comparing [$^{18}$F]FMISO and [$^{18}$F]FDG uptake. Patients with different tumors ranging from those with a high prevalence of hypoxia (HNC, glioma) to those that are less frequently hypoxic (breast cancer) were analyzed for the accumulation of [$^{18}$F]FMISO (*right column*) and [$^{18}$F]FDG (*left column*) via PET scans. Representative images for both tracers show only a minor correlation between the overall tumor maximum standardized uptake value for FDG and hypoxic volume in patients with (**a**) HNC, (**b**) liposarcoma of the left posterior shoulder, (**c**) axillary metastases from left breast cancer, and (**d**) glioma of the right frontal region. Significant differences among the different tumor types could be observed, indicating discordance between hypoxia and glucose metabolism (Reprinted with kind permission by AACR from Rajendran et al. [52])

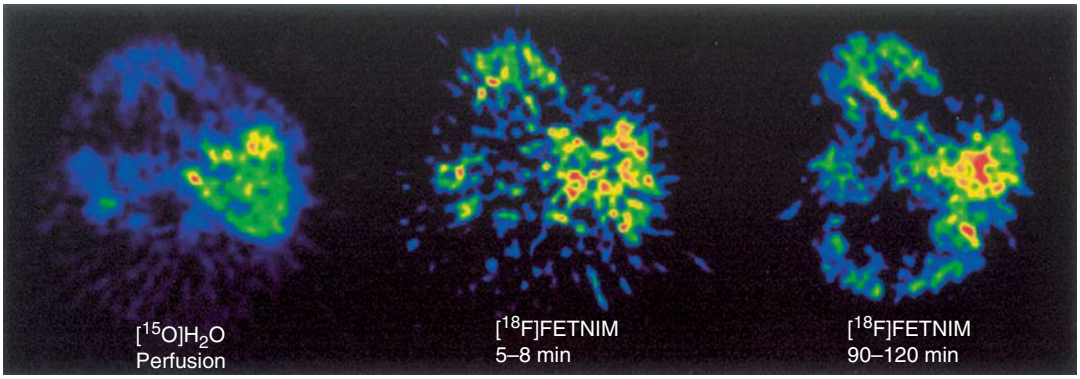


**Fig. 11.11** [18F]FETNIM uptake depends on the tumor perfusion. The tumor perfusion (assessed by [15O]$H_2O$ PET scan, *left*) of a patient with left hypopharyngeal tumor (HNC) was compared with a dynamic PET scan of [18F]FETNIM after 5–8 min (*middle*) and 90–120 min (*right*). The different pattern of [18F]FETNIM distribution in the early and late phases of the dynamic study depends on the perfusion of the tumor: At higher blood flow, the entrapment of [18F]FETNIM reflects the oxygenation well. The tissue-to-plasma ratios reached a steady-state level at 60 min p.i. in both tumor tissue and muscle indicating that the tissue-to-plasma ratio may provide best results using only a few late time points (The figure was reprinted with kind permission by Springer Science+Business Media from Lehtiö et al. [96])

tumors. In contrast to [18F]FMISO, however, [18F]FETNIM displayed a more favorable biodistribution with a low background signal in normoxic tissues [94]. This can be attributed to the higher hydrophilicity of [18F]FETNIM, enabling a higher tumor-to-background ratio. Clinical studies on [18F]FETNIM were performed with HNC patients in Finland, University of Turku. In these studies, it was shown that the early uptake of [18F]FETNIM was highly variable and depending on perfusion as demonstrated by [15$O_2$]$H_2O$ PET [95]. To monitor hypoxia, the tumor-to-plasma ratio provided the best results (Fig. 11.11) [96]. Especially at high blood flows, [18F]FETNIM accumulation reflects the oxygenation status well and thus should be well suited for hypoxia imaging in tissues with high blood flow. Assessing the radiotherapy response in 21 patients with HNC, a high uptake of [18F]FETNIM was shown to be related to a poor overall survival [97] underlining the predictive value of this hypoxia tracer. Also a preliminary study for 26 patients with NSCLC and a further with 16 cervical carcinoma patients provided evidence that [18F]FETNIM PET imaging is a valuable method to estimate hypoxia within tumors and to predict the overall survival of patients [98, 99].

Despite the promising results of [18F]FETNIM, further studies are required to validate this PET tracer as a noninvasive imaging agent for PET imaging. Furthermore, it remains to be determined whether the use of this PET tracer presents any advantages over the use of [18F]FMISO.

#### 11.2.2.3 [18F]Fluoroazomycin Arabinoside ([18F]FAZA)

[18F]Fluoroazomycin arabinoside [18F]FAZA (Fig. 11.3) exhibits superior pharmacokinetics compared to [18F]FMISO resulting from its reduced lipophilicity. This enables a faster clearance and hence a better contrast in imaging [100]. Additionally, [18F]FAZA can diffuse faster into cells so that this tracer is more readily available for hypoxic alteration [101, 102]. These observations are in line with a comparative study for [18F]FMISO and [18F]FAZA in mouse xenograft models where [18F]FAZA revealed better biokinetics with a higher tumor-to-muscle ratio and an oxygen-dependent uptake mechanism [103]. In contrast, a study published by Sorger et al. led to the conclusion that while [18F]FAZA indicates reduced oxygen levels comparable to [18F]FMISO in vitro, in vivo in a Walker 256 rat sarcoma model [18F]FMISO displayed a slightly higher uptake and tumor-to-muscle ratio [104]. To prove the superiority of [18F]FAZA over [18F]FMISO, more studies have to be undertaken. A further animal study with three squamous cell

carcinomas and one fibrosarcoma with differing characteristics regarding vascularization, hypoxia, and necrosis compared [$^{18}$F]FAZA uptake with Eppendorf electrode measurements and the hypoxia marker pimonidazole [105]. In vivo, the hypoxia selectivity of [$^{18}$F]FAZA could be proven in this study as well as in a study published by Tran et al. comparing OxyLite, EPR oximetry, and [$^{19}$F]MRI relaxometry [106].

Applying a chemoradiotherapy with tirapazamine – a prodrug activated to a toxic radical in hypoxic cells – the predictive value of [$^{18}$F]FAZA was investigated in a breast cancer xenograft-bearing tumor mouse model [107]. A high tumor accumulation of [$^{18}$F]FAZA was found to be an adverse indicator for tumor progression. Furthermore, [$^{18}$F]FAZA uptake could also predict the success of chemoradiotherapy, whereby the application of tirapazamine in hypoxic tumors could efficiently improve the therapeutic effect depending on the degree of hypoxia. The authors conclude that [$^{18}$F]FAZA prior to treatment might be a way to personalize tumor therapies involving radiation [107]. In these tumor-bearing mice also the reproducibility of hypoxia PET scans could be demonstrated. Therefore, pretreatment imaging is a valuable and reliable tool for treatment schemes targeting or modifying hypoxia [108].

In clinical studies, the feasibility of [$^{18}$F]FAZA was determined in 11 untreated HNC patients and 14 advanced rectal cancer patients [109, 110]. The quality of images achieved was adequate and the imaging feasible. The imaging for clinical static PET was performed 2 h p.i. and the recommended threshold was 1.5. [$^{18}$F]FAZA tumor uptake differed inter- and intraindividually; thus, further studies were undertaken to evaluate [$^{18}$F]FAZA in clinical settings. A study including 50 patients with different tumor entities confirmed the previously obtained data of [$^{18}$F]FAZA as feasible hypoxia tracer providing an adequate image quality [111]. The results of the DAHANCA (Danish Head and Neck Cancer Group) 24 trial including 50 patients revealed that in HNC patients receiving radiotherapy, [$^{18}$F]FAZA PET/CT was a prognostic factor regarding disease-free survival. Significant differences could be found between patients with and without hypoxic areas within their tumors [112].

Furthermore, the role of [$^{18}$F]FAZA PET imaging was analyzed in order to characterize hypoxia in the course of radiation treatment planning (Fig. 11.12) [83]. Eighteen patients with advanced squamous cell HNC were monitored, and the [$^{18}$F]FAZA uptake measurements were feasible for radiation treatment planning and IMRT (Sect. 11.4).

[$^{124}$I]iodoazomycinarabinoside ([$^{124}$I]IAZA) is an iodinated [$^{18}$F]FAZA analogue. As iodine has a longer half-life (4.18 days) than $^{18}$F (110 min), it was suggested that imaging at later time points might reveal advantages in imaging results. However, this could not be shown [100]. Instead, a deiodination of the molecule was suggested as a significant thyroid uptake was observed.

#### 11.2.2.4 [$^{18}$F]Fluoroetanidazole ([$^{18}$F]FETA)

[$^{18}$F]Fluoroetanidazole ([$^{18}$F]FETA) (Fig. 11.3) was first synthesized by Tewson in 1997 [113]. This nitroimidazole tracer has a decreased lipophilicity and superior biokinetics than [$^{18}$F]FMISO. In vivo, it turned out to be stable to nonhypoxic degradation and showed less metabolites in blood and urine compared to [$^{18}$F]FMISO. Preclinical studies with different tumor models showed that the uptake of [$^{18}$F]FETA correlates with the oxygen partial pressure within the tumor and a decrease in tracer uptake after carbogen breathing [114, 115]. The clinical potential of this promising PET hypoxia tracer has so far not been analyzed.

#### 11.2.2.5 2-(2-Nitro-1H-imidazol-1-yl)-*N*-(2,2,3,3,3-[$^{18}$F]pentafluoropropyl)-acetamide ([$^{18}$F]EF5)

Next to the mono-fluorinated 2-nitroimidazoles also fluoroalkylacetamide derivatives which are more highly fluorinated have been developed and named as EF1 [116], EF3 [117], and EF5 [118]. Among these, 2-(2-nitro-1H-imidazol-1-yl)-*N*-(2,2,3,3,3-[$^{18}$F]pentafluoropropyl)-acetamide (EF5) (Fig. 11.3) was originally developed as an agent for biopsy stainings and has only recently been introduced as PET tracer to monitor hypoxia. The biological half-life of this molecule is improved because of its enhanced lipophilicity [119]. So far, EF5 is the most stable 2-nitroimidazole reported [43].

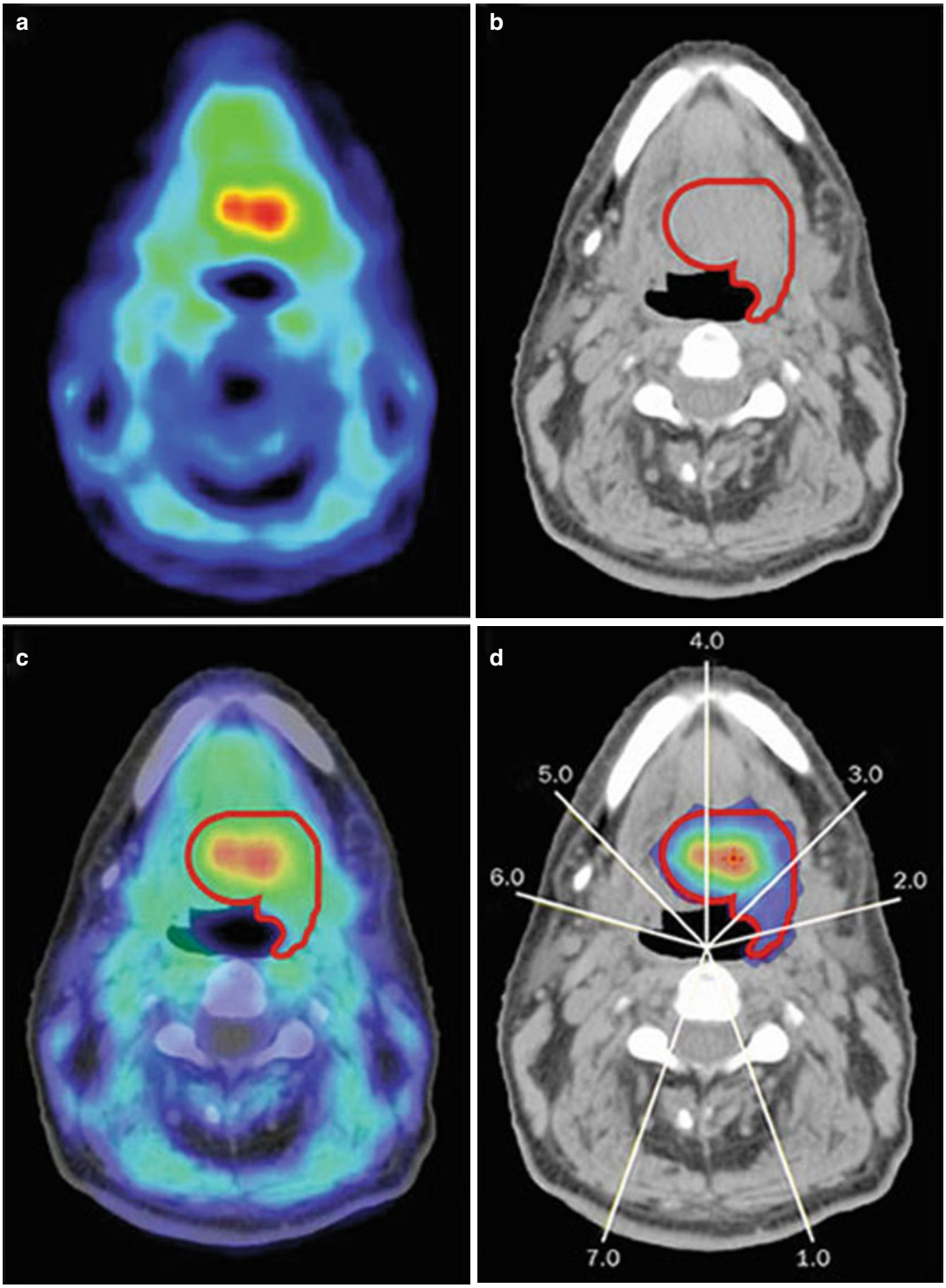


**Fig. 11.12** Use of [$^{18}$F]FAZA PET scans for dose painting. (**a**) The PET scan shows the uptake of [$^{18}$F]FAZA in an HNC patient with squamous cell carcinoma indicating hypoxic areas, (**b**) while the CT scan can be used to determine the GTV and hence for treatment planning and dose calculation. (**c**) If the PET and CT scans are fused, the exact localization of the hypoxic areas within the tumor can be determined and (**d**) dose distribution for dose-painting IMRT can be planned. The white lines indicate the direction of the radiation treatment fields resulting in the different doses for therapy (*blue*: 63 Gy, *red*: 98 Gy) (Reprinted by permission from Macmillan Publishers Ltd: Horsman, 2012, © 2012, Nature Publishing group [45])

The major limitation of this promising agent is the more complex labeling chemistry based on electrophilic fluorination that hampers its availability in comparison to the nucleophilic displacement reactions used in the radiosynthesis of the mono-fluorinated 2-nitroimidazoles [120].

The first human trial was performed on 15 HNC patients whereby the feasibility of [$^{18}$F]EF5 could be demonstrated. In a time course analysis, Komar et al. demonstrated a blood-flow-dependent initial distribution which showed to be hypoxia-specific at later time points. The best results were found performing the PET scan 3 h p.i. with a tumor-to-muscle cutoff value of 1.5 (Fig. 11.13) [121]. Additionally, [$^{18}$F]EF5 reveals a predictive value as an increased tumor uptake

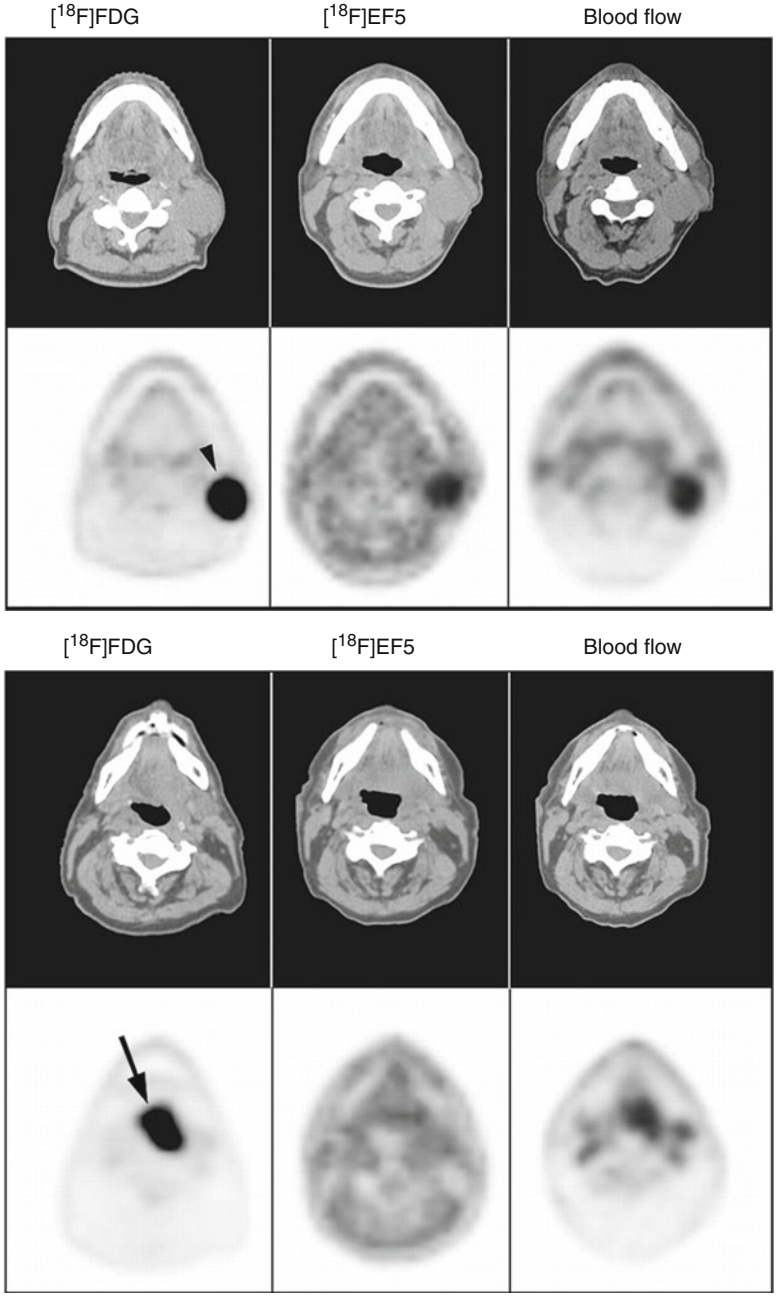


**Fig. 11.13** Comparison of PET/CT scans for [$^{18}$F]EF5, [$^{18}$F]FDG, and [$^{15}$O]$H_2O$. In three squamous cell HNC patients, the three tracers [$^{18}$F]EF5, [$^{18}$F]FDG, and [$^{15}$O]$H_2O$ were applied and PET/CT scans performed. The measurement of blood flow was followed by an [$^{18}$F]EF5 PET/CT scan. The [$^{18}$F]FDG scan was performed separately. The primary and metastatic lesions are visible on the blood flow and the [$^{18}$F]FDG scans. [$^{18}$F]EF5 PET was measured 3 h p.i. This tracer detects hypoxia well in HNC patients. Voxel-by-voxel analysis of co-registered blood flow and [$^{18}$F]EF5 revealed a distinct pattern of hypoxia with a tumor-to-muscle ratio of 1.5 at 3 h for clinically significant hypoxia. The three tracers did not show a significant correlation although a negative relationship between [$^{15}$O]$H_2O$ and [$^{18}$F]EF5 could be detected. While *arrows* indicate primary tumors, *arrowheads* point to metastatic lesions (Reprinted by permission of SNMMI from: Komar et al. [121])

**Fig. 11.13** (continued)

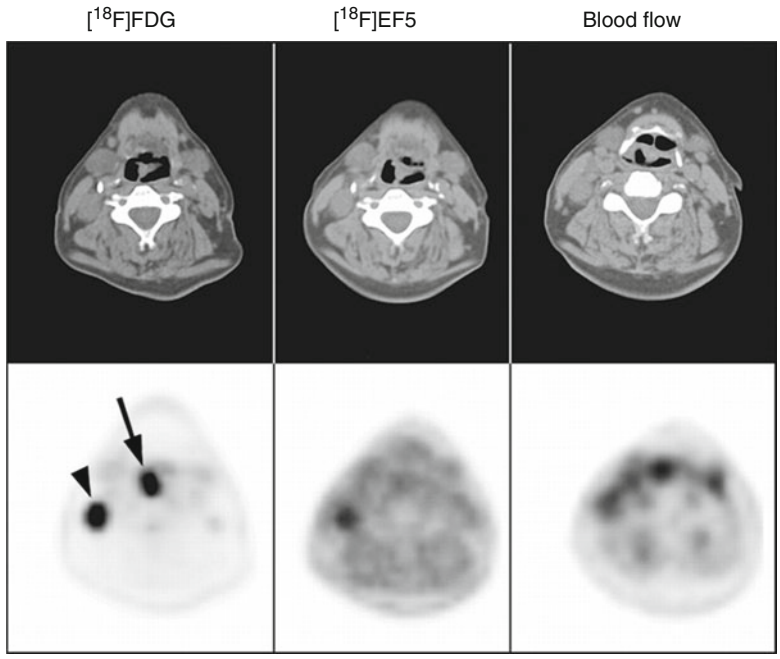


correlates with higher grade tumors and a high prevalence of metastasis formation [122, 123].

A comparative study with [18F]EF3 and [18F]FDG was performed in patients with HNC [119]. No correlation in the uptake of the two tracers could be observed underlining the difference of the hypoxia-specific [18F]EF3 and the tumor-sensitive [18F]FDG.

### 11.2.3 Cu-Diacetyl-bis($N^4$-methylthiosemicarbazone) (Cu-ATSM)

An alternative agent with great promise for PET hypoxia imaging is Cu-diacetyl-bis($N^4$-methylthiosemicarbazone) (Cu-ATSM) developed from the blood perfusion agent Cu-pyruvaldehyde-bis($N^4$-methylthiosemicarbazone) (Cu-PTSM) [124]. Cu-ATSM consists of the chelator diacetyl-bis($N^4$-methylthiosemicarbazone) complexing a copper(II) ion (Fig. 11.14). The precursor can be rapidly labeled with a variety of copper isotopes. The four positron-emitting radioisotopes Cu-60 ($t_{1/2}$ 0.4 h), Cu-61 ($t_{1/2}$ 3.32 h), Cu-62 ($t_{1/2}$ 0.16 h), and Cu-64 ($t_{1/2}$ 12.7 h) can be used flexibly for PET imaging [125] and

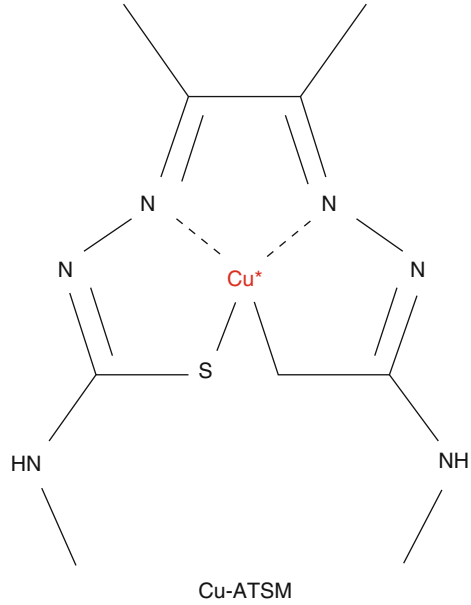


**Fig. 11.14** Structure of Cu-ATSM. The highlighted Cu ion (Cu*) is a representation of the radioactive isotopes Cu-60, Cu-61, Cu-62, and Cu-64

serial imaging can be performed in short intervals to monitor reperfusion using the short-lived radionuclides [69]. Cu-ATSM is retained in higher extent (up to tenfold) than [18F]FMISO

within hypoxic cells as demonstrated for EMT6 breast cancer cells [126]. The neutral lipophilic molecule is highly membrane permeable and can pass normoxic cells metabolically unchanged due to its relatively low redox potential. Cu(II)-ATSM is retained comparable to the nitroimidazoles in hypoxic tissues following its reduction to $[Cu(I)\text{-}ATSM]^-$ due to its negative charge. The exact mechanism of how Cu-ATSM is entrapped within cells is however not completely understood. It is suggested that the reduction of Cu(II) ATSM is a reversible process in the presence of oxygen. Furthermore, it is hypothesized that Cu(I) might dissociate slowly and irreversibly from the complex which could explain the only partial washout of copper isotopes after the reoxygenation of cells [127].

Several studies have been undertaken to preclinically evaluate the value of Cu-ATSM in hypoxia imaging. An in vivo glioma xenograft model demonstrated the correlation of Cu-ATSM and partial oxygen pressure within the tumor in comparison to polarographic electrode measurements [128]. Due to its high background clearance, Cu-ATSM results in a higher signal-to-noise ratio [129] although also an unspecific retention could be observed [130]. Compared to nitroimidazoles, Cu-ATSM showed higher tumor uptakes resulting in high-quality images at 20 min p.i. [126, 128]. A study comparing [$^{18}$F]EF5 with [$^{64}$Cu]ATSM in fibrosarcomas, 9L glioma, and animal R3230 mammary adenocarcinomas demonstrated Cu-ATSM to be a valuable hypoxia marker in some tumor types but not for all [130]. In some tumor cell lines like FSA rat fibrosarcoma [130], R3327-AT rat prostatic [131], and SCCVII murine squamous cell carcinoma [132], no significant correlation between hypoxia and tracer accumulation could be observed. This intertumoral selectivity remains one of the main challenges for the use of Cu-ATSM as a general hypoxia marker. Different hypotheses exist concerning the varying retention within hypoxic cells. On the one hand, different redox potentials might explain for the differences as well as the pH within the cells [133], and on the other hand, it is presumed that Cu(I) dissociating from Cu-ATSM might be transported out of the tumor cells as the copper transporter ATP7B could be shown to be overexpressed in several human malignancies, e.g., in breast, ovarian, and gastric cancer [134].

[$^{60}$Cu]ATSM has been validated for its use especially for cervical and lung cancers. The appropriate threshold to discriminate between hypoxia and normoxic tissue was determined to be 3.5 after a dynamic imaging for 60 min in 14 patients with biopsy-proven cervical cancer [135]. These results could be confirmed in a second study with 38 patients with cervical cancer [136]. The uptake of [$^{60}$Cu]ATSM furthermore proved to be predictive for progression-free survival and overall survival. In both studies no correlation with FDG uptake could be observed. The ACRIN (American College of Radiology Imaging Network) trial 6682 is currently ongoing with the aim to assess the potential of [$^{64}$Cu] ATSM as predictive biomarker for treatment outcome in cervical cancer in 100 female participants [44].

In further clinical settings, the predictive role for [$^{60}$Cu]ATSM could be demonstrated. In an initial study with 14 patients with biopsy-proven non-small cell lung cancer, the [$^{60}$Cu]ATSM uptake correlated with the therapy response to radiation or chemotherapy, discriminating responders from nonresponders (Fig. 11.15) [137]. In 2008, Dietz and collaborators showed in a pilot study that [$^{60}$Cu]ATSM may be predictive of survival and tumor response to neoadjuvant chemoradiotherapy in patients with locally invasive primary or node-positive rectal cancer [138]. Semiquantitatively, the tumor uptake of the PET tracer was determined using the tumor-to-muscle ratio. If this ratio exceeded 2.6, patients had a worse prognosis regarding the overall and progression-free survival. An increase of the molecular hypoxia markers VEGF, EGFR, COX-2, and CAIX, an increase in apoptosis, as well as a poor outcome could be shown to be associated with [$^{60}$Cu]ATSM uptake in cervical cancer patients [135].

Also for IMRT, Cu-ATSM imaging via PET/CT might prove feasible as shown by Chao and collaborators for patients with HNC [139].

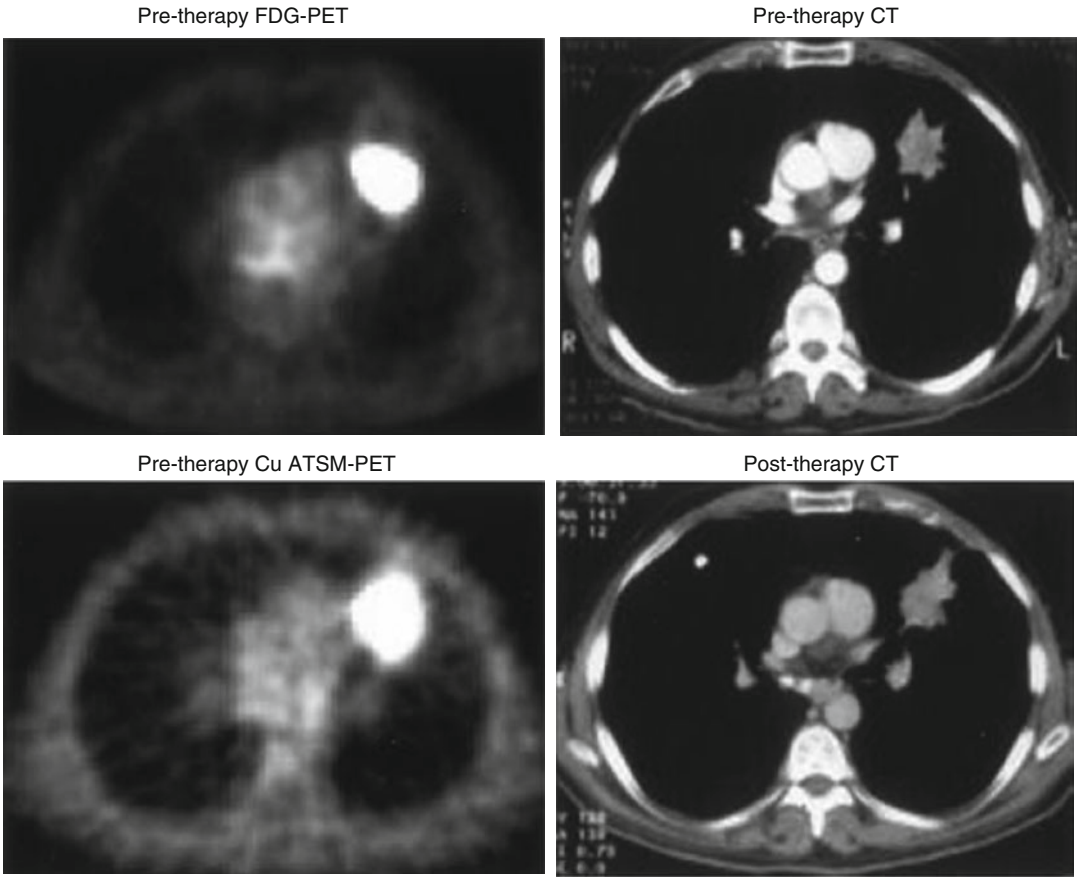


**Fig. 11.15** Feasibility of [$^{60}$Cu]ATSM in clinical imaging of NSCLC for predicting the response to therapy. The pre-therapy [$^{18}$F]FDG-PET scan (*upper left*) and the CT scan (*upper right*) of this NSCLC patient representing the results of a nonresponder confirm the existence of the tumor in the lingular mass. The uptake of [$^{60}$Cu]ATSM was analyzed prior to therapy using PET scan (*lower left*) and compared to tumor response to therapy. Nonresponders had a tumor-to-muscle ratio of ≥3.0. The PET results were correlated with a follow-up PET scan 3 months after chemotherapy. The patient died 15 months after diagnosis due to progressive disease. [$^{18}$F]FDG uptake and responsiveness to therapy as well as [$^{18}$F]FDG and [$^{60}$Cu]ATSM uptake did not correlate significantly (The figure was reprinted with kind permission by Springer Science+Business Media from Dehdashti et al. [137])

In summary, Cu-ATSM holds promise for the future PET imaging irrespective of the applied copper isotope [140]. Due to its small molecular weight and high membrane permeability, it shows a high diffusion rate into cells where it is rapidly reduced and retained in case of hypoxia. Cu-ATSM might also respond to other adverse conditions within the tumor indicating that Cu-ATSM might be a more general biomarker for poor treatment response [44]. Furthermore, Cu-ATSM exhibits a high tumor-to-background ratio as it is cleared fast from the blood. Positive results in future clinical applications are thus to be expected [61].

### 11.2.4 Anti-Carbonic Anhydrase IX (CAIX) Antibodies

Another strategy for the detection of hypoxia via PET depends on the radiolabeling of anti-carbonic anhydrase IX (CAIX) antibodies. One

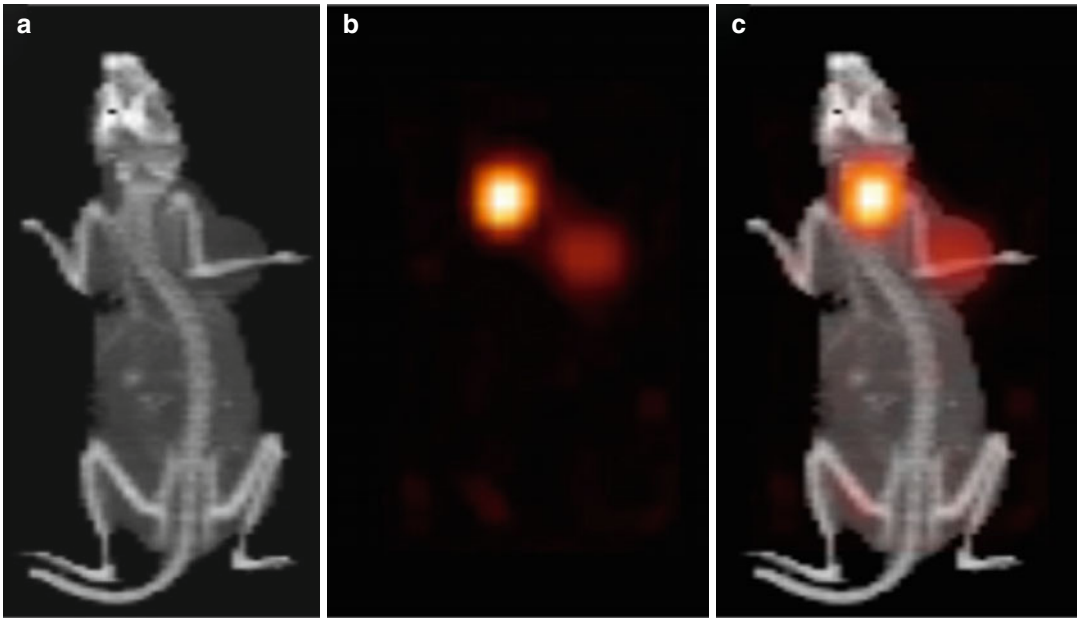


**Fig. 11.16** Uptake of the anti-CAIX antibody [$^{124}$I]cG250 in xenografted RCC. At day 3 p.i., [$^{124}$I]cG250 accumulates with a maximal trend towards correlation to the partial oxygen pressure within the xenografted RCC SK-RC 52 in balb/c nude mice. (**a**) The CT scan visualizes the localization of the xenograft in the right shoulder region, (**b**) whereas the localization of [$^{124}$I]cG250 can be observed in the PET scan. Liberated [$^{124}$I] is retained in the thyroid. (**c**) The co-registered [$^{124}$I]cG250 PET/CT scan demonstrates the better imaging of multiparametric assessments (Reprinted with permission by Elsevier from Lawrentschuk et al. [147])

of the downstream targets of the transcription factor HIF-1α is CAIX which is upregulated under hypoxic conditions and hence an intrinsic hypoxia-related (endogenous) cell marker [141, 142]. This enzyme is displayed on the cell surface of hypoxic cells [141], while normoxic cells of the gastric mucosa, bile ducts, and small intestine show only a basal expression of CAIX. After determination of the CAIX levels within hypoxic areas, the treatment of patients with CAIX-targeted therapeutics could also be favorable.

A study with fragments of the anti-CAIX antibody cG250 was undertaken in order to investigate the assessment of tumor hypoxia in a tumor xenograft model of a human HNC and to determine the spatial correlation between radiotracer to the microscopic distribution of the cells [143]. The [$^{89}$Zr]cG250(Fab′)$_2$ uptake correlated significantly and rapidly after injection with the immunohistochemical staining for CAIX expression, and tumors could be clearly visualized by PET after 4 h. 24 h p.i., the tumor uptake was already reduced, displaying presumably the fast pharmacodynamics of the tracer. In comparison to pimonidazole staining, however, the signal of the antibody fragments was reduced.

As a significant molecular marker, 87–100 % of the clear cell subtype of renal cell carcinoma (RCC) express CAIX [144–146]. Hence, a further study to detect hypoxia in a human xenograft model of RCC was undertaken with [$^{124}$I]cG250 [147]. All tumors analyzed developed hypoxia and the antibody localized in excellent manner within the tumors as measured by PET/CT correlating to the obtained data of polarographic $O_2$ microelectrode probes (Fig. 11.16). However, no significant correlation between the expression of CAIX and hypoxia could be found. This might be due to the fact that CAIX is also involved in angiogenesis which occurs throughout the tumor.

As these results for the antibody and fragments of cG250 are holding great promise, further studies are warranted to verify their value in the imaging of hypoxia.

## 11.3 Integrin-Specific PET Tracers: An Indirect Marker for Tumor Hypoxia?

Angiogenesis is a central hallmark of tumors reaching a size of more than ~1 $mm^3$ [148]. Hypoxia leads to angiogenesis as the transcription factor HIF-1 upregulates the expression of VEGF, PDGFB, and other critical angiogenic growth factors [149]. Angiogenesis is a potential target for cancer diagnosis and therapy, and hence, research focuses on it on a basal, translational, and clinical level. Integrin $\alpha_v\beta_3$ playing a central role in angiogenesis is expressed on the surface of activated endothelial cells and is furthermore also under the control of HIF-1 [150]. Therefore, integrin-targeted PET tracers like RGD derivatives labeled with $^{18}F$ and $^{68}Ga$ might also be useful in hypoxia detection. The data obtained from studies trying to correlate the distribution of hypoxia and integrin markers did not come to conclusive results [151, 152]. One major drawback of this angiogenesis imaging is that integrins can be detected on all cells throughout the tumor and that they are not hypoxia-specific. Further research is required to clarify the connection of hypoxia and angiogenesis. Nevertheless, the imaging of these two parameters might help tailoring individual tumor therapies.

## 11.4 Treatment Planning in Therapy After Hypoxia PET Imaging

Although limited in treatment response, hypoxic areas within tumors harbor the opportunity for tumor selective therapies including prodrugs activated by hypoxia, hypoxia-specific gene therapy, or targeting molecules upon which hypoxic cell survival depends [153]. Ideally, the development of novel bioreductive therapeutics with a paired diagnostic value will be forced [4]. Oncology has to exploit this highly validated target for therapy [4]. Furthermore, in radiation therapy IMRT can be applied after determining hypoxic areas within a tumor enabling dose escalation during radiation therapies. In a so-called dose-painting process, the dose delivered to the hypoxic tissues can be individually adapted in order to overcome radiation resistance depending on the severity of hypoxia [154]. Dose painting describes the administration of a nonuniform radiation dose distribution in the target volume which is based on functional or molecular images [155]. Yet the feasibility of IMRT has to be evaluated in clinical settings.

The main goal of radiation therapies is to destroy in a local treatment all tumor cells and to achieve a complete remission. The sparing of healthy tissues while destroying a maximum of the tumor via dose escalation is another objective aiming at a greater tumor control with lower side effects. The dependence of radiation resistance on hypoxia is well known and might be overcome by dose escalation in the hypoxic areas after detection. Currently no study describes the improvement of outcome after enhancing the radiation dose to hypoxic tissues. For treatment planning in radiation therapy, PET imaging exhibits some limitations which have to be overcome. Usually, clinical PET scanners have a resolution of about 2–4 mm, while the hypoxic areas within a tumor can exhibit dimensions of some 100 μm [105, 156]. Therefore, only "partial volume effects" can be measured as one voxel might contain regions of normoxia as well as extreme hypoxia (Fig. 11.17). Additionally, also background noise, patient movements, and the tumor as dynamic system itself might modulate the intensities leading to irregularities and ambiguities in the PET signal. At a subvoxel scale the severity of hypoxia and the resulting level of radiosensitivity cannot be determined. Therefore, multiparametric imaging combining MRI (BOLD) with PET as well as dynamic imaging might yield a better and synergistically optimized representation of the actual tumor biology [41]. Another unresolved question so far is the influence of increased radiation applied to the tissues. Nevertheless, dose painting seems to be a realistic and attractive concept which needs to be clinically proven.

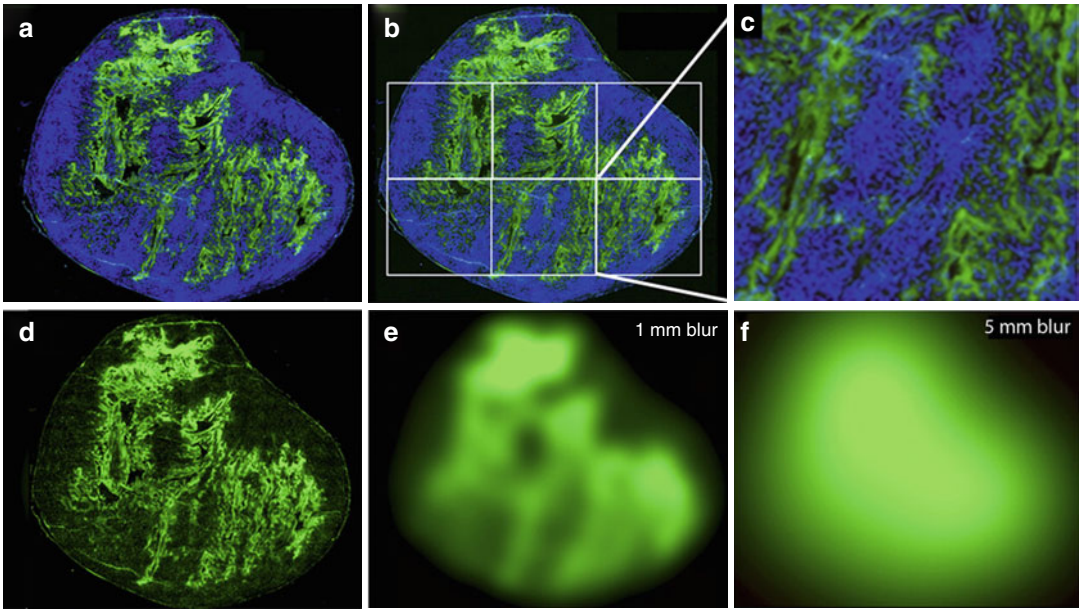


**Fig. 11.17** Comparison of the resolution of hypoxia detection using immunohistochemistry to PET imaging. (**a**) A histologic section of a tumor was stained with the hypoxia marker pimonidazole (*green*) and the vascular perfusion marker Hoechst 33342 (*blue*) demonstrating the dispersed hypoxic areas within the tumor. (**b**) The superimposition of the same image with six 5 $mm^2$ regions represents the resolution of a clinical PET scanner (**c**) where single regions can be magnified and analyzed. (**d**–**f**) If for the same image stained solely with pimonidazole a Gaussian blur of 1 mm (**e**) and 5 mm (**f**) is applied, the resolution of clinical PET scanners is obtained. These pictures clearly indicate the dependence of voxel values on the maximum uptake of tracer and the hypoxic fraction of voxels. The signals are averaged. If the spatial resolution is increased, the hypoxic areas can be visualized with a higher reliability playing an important role in radiotherapy planning using IMRT (Reprinted by permission of SNMMI from Carlin and Humm [44])

## Conclusion

Several PET tracers for the noninvasive detection of hypoxia have been developed and investigated to predict the outcome and identify patients with an impaired prognosis due to hypoxia. The application of hypoxia tracers for PET and PET/CT provides so far a useful and informative value for the prognosis of rectal and cervical carcinoma, NSCLC, glioma, and head and neck tumors. Unfortunately, the imaging contrast in comparison to [$^{18}$F]FDG is relatively low and impedes the analysis. The establishment and validation of hypoxia PET tracers is still under development, and the clinical use of these agents depends on how reliable their predictive value will prove to be. Nevertheless, PET, PET/CT, and PET/MRI offer the potential to optimize and individualize the treatments of patients suffering from hypoxic cancers. The risk stratification of newly diagnosed tumors as well as tailored treatment could be possible using dose escalation and dose painting in radiotherapy as well as hypoxia-activated drugs. The road to personalized medicine requires molecular imaging beyond tumor detection as also the characterization of the tumor on a functional level is of critical importance.

## References

1. West JB. Respiratory physiology – the essentials. Baltimore/London/Los Angeles: Williams & Wilkins; 1999.
2. Helmlinger G, et al. Interstitial pH and pO2 gradients in solid tumors in vivo: high-resolution measurements reveal a lack of correlation. Nat Med. 1997;3:177–82.
3. Vaupel P, et al. Blood flow, tissue oxygenation, pH distribution, and energy metabolism of murine mammary adenocarcinomas during growth. Adv Exp Med Biol. 1989;248:835–45.

4. Wilson WR, Hay MP. Targeting hypoxia in cancer therapy. Nat Rev Cancer. 2011;11:393–410.
5. Höckel M, Vaupel P. Tumor hypoxia: definitions and current clinical, biologic, and molecular aspects. J Natl Cancer Inst. 2001;93:266–76.
6. Vaupel P, Harrison L. Tumor hypoxia: causative factors, compensatory mechanisms, and cellular response. Oncologist. 2004;9 Suppl 5:4–9.
7. Vaupel P, Mayer A. Hypoxia in cancer: significance and impact on clinical outcome. Cancer Metastasis Rev. 2007;26:225–39.
8. Boyer PD, et al. Oxidative phosphorylation and photophosphorylation. Annu Rev Biochem. 1977;46: 955–66.
9. Honig CR. Modern cardiovascular physiology. Boston/Toronto: Little and Brown; 1988.
10. Zander R, Vaupel P. Proposal for using a standardized terminology on oxygen transport to tissue. Adv Exp Med Biol. 1985;191:965–70.
11. Crabtree HG, Cramer W. The action of radium on cancer cells. II. Some factors determining the susceptibility of cancer cells to radium. Proc R Soc Lond B. 1933;113:238–50.
12. Schwarz G. Desensibilisierung gegen Röntgen- und Radiumstrahlen. Münchener Med Wochenschau. 1909;24:1–2.
13. Gray LH, et al. The concentration of oxygen dissolved in tissues at the time of irradiation as a factor in radiotherapy. Br J Radiol. 1953;26:638–48.
14. Hall EJ. Radiobiology for the radiologist. Philadelphia: Lippincott; 1994.
15. Comerford KM, et al. Hypoxia-inducible factor-1-dependent regulation of the multidrug resistance (MDR1) gene. Cancer Res. 2002;62:3387–94.
16. Thews O, et al. Hypoxia-induced extracellular acidosis increases p-glycoprotein activity and chemoresistance in tumors in vivo via p38 signaling pathway. Adv Exp Med Biol. 2011;701:115–22.
17. Riva C, et al. Cellular physiology and molecular events in hypoxia-induced apoptosis. Anticancer Res. 1998;18:4729–36.
18. Shimizu S, et al. Prevention of hypoxia-induced cell death by Bcl-2 and Bcl-xL. Nature. 1995;374: 811–3.
19. Soengas MS, et al. Apaf-1 and caspase-9 in p53-dependent apoptosis and tumor inhibition. Science. 1999;284:156–9.
20. Giaccia AJ. Hypoxic stress proteins: survival of the fittest. Semin Radiat Oncol. 1996;6:46–58.
21. Koch CJ, et al. The effect of hypoxia on the generation time of mammalian cells. Radiat Res. 1973;53:43–8.
22. Pettersen EO, Lindmo T. Inhibition of cell-cycle progression by acute treatment with various degrees of hypoxia: modifications induced by low concentrations of misonidazole present during hypoxia. Br J Cancer. 1983;48:809–17.
23. Yuan J, Glazer PM. Mutagenesis induced by the tumor microenvironment. Mutat Res. 1998;400: 439–46.
24. Harris AL. Hypoxia – a key regulatory factor in tumour growth. Nat Rev Cancer. 2002;2:38–47.
25. Pennacchietti S, et al. Hypoxia promotes invasive growth by transcriptional activation of the met protooncogene. Cancer Cell. 2003;3:347–61.
26. Kang SS, et al. Clinical significance of glucose transporter 1 (GLUT1) expression in human breast carcinoma. Jpn J Cancer Res. 2002;93:1123–8.
27. Kunkel M, et al. Overexpression of Glut-1 and increased glucose metabolism in tumors are associated with a poor prognosis in patients with oral squamous cell carcinoma. Cancer. 2003;97:1015–24.
28. Younes M, et al. Overexpression of Glut1 and Glut3 in stage I nonsmall cell lung carcinoma is associated with poor survival. Cancer. 1997;80:1046–51.
29. Parkkila S, et al. Carbonic anhydrase inhibitor suppresses invasion of renal cancer cells in vitro. Proc Natl Acad Sci U S A. 2000;97:2220–4.
30. Robertson N, et al. Role of carbonic anhydrase IX in human tumor cell growth, survival, and invasion. Cancer Res. 2004;64:6160–5.
31. Weinberg RA. The biology of cancer. New York/Abingdon: Garland Science; 2007.
32. Aebersold DM, et al. Expression of hypoxia-inducible factor-1alpha: a novel predictive and prognostic parameter in the radiotherapy of oropharyngeal cancer. Cancer Res. 2001;61:2911–6.
33. Bos R, et al. Levels of hypoxia-inducible factor-1alpha independently predict prognosis in patients with lymph node negative breast carcinoma. Cancer. 2003;97:1573–81.
34. Griffiths EA, et al. Hypoxia-inducible factor-1alpha expression in the gastric carcinogenesis sequence and its prognostic role in gastric and gastro-oesophageal adenocarcinomas. Br J Cancer. 2007;96:95–103.
35. Swinson DE, et al. Hypoxia-inducible factor-1 alpha in non small cell lung cancer: relation to growth factor, protease and apoptosis pathways. Int J Cancer. 2004;111:43–50.
36. Trastour C, et al. HIF-1alpha and CA IX staining in invasive breast carcinomas: prognosis and treatment outcome. Int J Cancer. 2007;120:1451–8.
37. Vleugel MM, et al. Differential prognostic impact of hypoxia induced and diffuse HIF-1alpha expression in invasive breast cancer. J Clin Pathol. 2005;58:172–7.
38. Jubb AM, et al. Assessment of tumour hypoxia for prediction of response to therapy and cancer prognosis. J Cell Mol Med. 2010;14:18–29.
39. Semenza GL. Targeting HIF-1 for cancer therapy. Nat Rev Cancer. 2003;3:721–32.
40. Krause BJ, et al. PET and PET/CT studies of tumor tissue oxygenation. Q J Nucl Med Mol Imaging. 2006;50:28–43.
41. Thorwarth D, Alber M. Implementation of hypoxia imaging into treatment planning and delivery. Radiother Oncol. 2010;97:172–5.
42. Astner ST, et al. Imaging of tumor physiology: impacts on clinical radiation oncology. Exp Oncol. 2010;32:149–52.

43. Lapi SE, et al. Positron emission tomography imaging of hypoxia. PET Clin. 2009;4:39–47.
44. Carlin S, Humm JL. PET of hypoxia: current and future perspectives. J Nucl Med. 2012;53:1171–4.
45. Horsman MR, et al. Imaging hypoxia to improve radiotherapy outcome. Nat Rev Clin Oncol. 2012;9:674–87.
46. Semenza GL. HIF-1: upstream and downstream of cancer metabolism. Curr Opin Genet Dev. 2010;20:51–6.
47. Busk M, et al. Cellular uptake of PET tracers of glucose metabolism and hypoxia and their linkage. Eur J Nucl Med Mol Imaging. 2008;35:2294–303.
48. Cherk MH, et al. Lack of correlation of hypoxic cell fraction and angiogenesis with glucose metabolic rate in non-small cell lung cancer assessed by 18F-fluoromisonidazole and 18F-FDG PET. J Nucl Med. 2006;47:1921–6.
49. Eschmann SM, et al. Prognostic impact of hypoxia imaging with 18F-misonidazole PET in non-small cell lung cancer and head and neck cancer before radiotherapy. J Nucl Med. 2005;46:253–60.
50. Gagel B, et al. [18F] fluoromisonidazole and [18F] fluorodeoxyglucose positron emission tomography in response evaluation after chemo-/radiotherapy of non-small-cell lung cancer: a feasibility study. BMC Cancer. 2006;6:51.
51. Rajendran JG, et al. [(18)F]FMISO and [(18)F]FDG PET imaging in soft tissue sarcomas: correlation of hypoxia, metabolism and VEGF expression. Eur J Nucl Med Mol Imaging. 2003;30:695–704.
52. Rajendran JG, et al. Hypoxia and glucose metabolism in malignant tumors: evaluation by [18F]fluoromisonidazole and [18F]fluorodeoxyglucose positron emission tomography imaging. Clin Cancer Res. 2004;10:2245–52.
53. Thorwarth D, et al. Combined uptake of [18F]FDG and [18F]FMISO correlates with radiation therapy outcome in head-and-neck cancer patients. Radiother Oncol. 2006;80:151–6.
54. Chapman JD. Hypoxic sensitizers – implications for radiation therapy. N Engl J Med. 1979;301:1429–32.
55. Chapman JD, et al. A marker for hypoxic cells in tumours with potential clinical applicability. Br J Cancer. 1981;43:546–50.
56. Brown JM. Clinical trials of radiosensitizers: what should we expect? Int J Radiat Oncol Biol Phys. 1984;10:425–9.
57. Grunbaum Z, et al. Synthesis and characterization of congeners of misonidazole for imaging hypoxia. J Nucl Med. 1987;28:68–75.
58. Martin GV, et al. Noninvasive detection of hypoxic myocardium using fluorine-18-fluoromisonidazole and positron emission tomography. J Nucl Med. 1992;33:2202–8.
59. Prekeges JL, et al. Reduction of fluoromisonidazole, a new imaging agent for hypoxia. Biochem Pharmacol. 1991;42:2387–95.
60. Tatum JL, et al. Hypoxia: importance in tumor biology, noninvasive measurement by imaging, and value of its measurement in the management of cancer therapy. Int J Radiat Biol. 2006;82:699–757.
61. Mees G, et al. Molecular imaging of hypoxia with radiolabelled agents. Eur J Nucl Med Mol Imaging. 2009;36:1674–86.
62. Whitmore GF, Varghese AJ. The biological properties of reduced nitroheterocyclics and possible underlying biochemical mechanisms. Biochem Pharmacol. 1986;35:97–103.
63. Rasey JS, et al. Comparison of binding of [3H]misonidazole and [14C]misonidazole in multicell spheroids. Radiat Res. 1985;101:473–9.
64. Rasey JS, et al. Characterization of radiolabeled fluoromisonidazole as a probe for hypoxic cells. Radiat Res. 1987;111:292–304.
65. Krohn KA, et al. Molecular imaging of hypoxia. J Nucl Med. 2008;49 Suppl 2:129S–48.
66. Padhani A. PET imaging of tumour hypoxia. Cancer Imaging. 2006;6:S117–21.
67. Graham MM, et al. Fluorine-18-fluoromisonidazole radiation dosimetry in imaging studies. J Nucl Med. 1997;38:1631–6.
68. Overgaard J. Clinical evaluation of nitroimidazoles as modifiers of hypoxia in solid tumors. Oncol Res. 1994;6:509–18.
69. Padhani AR, et al. Imaging oxygenation of human tumours. Eur Radiol. 2007;17:861–72.
70. Nunn A, et al. Nitroimidazoles and imaging hypoxia. Eur J Nucl Med. 1995;22:265–80.
71. Martin GV, et al. Fluoromisonidazole. A metabolic marker of myocyte hypoxia. Circ Res. 1990;67:240–4.
72. Piert M, et al. Introducing fluorine-18 fluoromisonidazole positron emission tomography for the localisation and quantification of pig liver hypoxia. Eur J Nucl Med. 1999;26:95–109.
73. Chang J, et al. A robotic system for 18F-FMISO PET-guided intratumoral pO2 measurements. Med Phys. 2009;36:5301–9.
74. Bentzen L, et al. Assessment of hypoxia in experimental mice tumours by [18F]fluoromisonidazole PET and pO2 electrode measurements. Influence of tumour volume and carbogen breathing. Acta Oncol. 2002;41:304–12.
75. Dubois L, et al. Evaluation of hypoxia in an experimental rat tumour model by [(18)F]fluoromisonidazole PET and immunohistochemistry. Br J Cancer. 2004;91:1947–54.
76. Troost EG, et al. Imaging hypoxia after oxygenation-modification: comparing [18F]FMISO autoradiography with pimonidazole immunohistochemistry in human xenograft tumors. Radiother Oncol. 2006;80:157–64.
77. Troost EG, et al. Correlation of [18F]FMISO autoradiography and pimonidazole [corrected] immunohistochemistry in human head and neck carcinoma xenografts. Eur J Nucl Med Mol Imaging. 2008;35:1803–11.
78. Rasey JS, et al. Quantifying hypoxia with radiolabeled fluoromisonidazole: pre-clinical and clinical

studies. In: Machulla H-J, editor. The imaging of hypoxia. Dordrecht: Kluwer Academic Publishers; 1999.
79. Gagel B, et al. pO(2) Polarography versus positron emission tomography ([(18)F] fluoromisonidazole, [(18)F]-2-fluoro-2′-deoxyglucose). An appraisal of radiotherapeutically relevant hypoxia. Strahlenther Onkol. 2004;180:616–22.
80. Zimny M, et al. FDG – a marker of tumour hypoxia? A comparison with [18F]fluoromisonidazole and pO2-polarography in metastatic head and neck cancer. Eur J Nucl Med Mol Imaging. 2006;33:1426–31.
81. Valk PE, et al. Hypoxia in human gliomas: demonstration by PET with fluorine-18-fluoromisonidazole. J Nucl Med. 1992;33:2133–7.
82. Rasey JS, et al. Quantifying regional hypoxia in human tumors with positron emission tomography of [18F]fluoromisonidazole: a pretherapy study of 37 patients. Int J Radiat Oncol Biol Phys. 1996;36:417–28.
83. Grosu AL, et al. Hypoxia imaging with FAZA-PET and theoretical considerations with regard to dose painting for individualization of radiotherapy in patients with head and neck cancer. Int J Radiat Oncol Biol Phys. 2007;69:541–51.
84. Spence AM, et al. Regional hypoxia in glioblastoma multiforme quantified with [18F]fluoromisonidazole positron emission tomography before radiotherapy: correlation with time to progression and survival. Clin Cancer Res. 2008;14:2623–30.
85. Bentzen L, et al. Tumour oxygenation assessed by 18F-fluoromisonidazole PET and polarographic needle electrodes in human soft tissue tumours. Radiother Oncol. 2003;67:339–44.
86. Lee NY, et al. Fluorine-18-labeled fluoromisonidazole positron emission and computed tomography-guided intensity-modulated radiotherapy for head and neck cancer: a feasibility study. Int J Radiat Oncol Biol Phys. 2008;70:2–13.
87. Lin Z, et al. The influence of changes in tumor hypoxia on dose-painting treatment plans based on 18F-FMISO positron emission tomography. Int J Radiat Oncol Biol Phys. 2008;70:1219–28.
88. Rischin D, et al. Prognostic significance of [18F]-misonidazole positron emission tomography-detected tumor hypoxia in patients with advanced head and neck cancer randomly assigned to chemoradiation with or without tirapazamine: a substudy of Trans-Tasman Radiation Oncology Group Study 98.02. J Clin Oncol. 2006;24:2098–104.
89. Jansen JF, et al. Noninvasive assessment of tumor microenvironment using dynamic contrast-enhanced magnetic resonance imaging and 18F-fluoromisonidazole positron emission tomography imaging in neck nodal metastases. Int J Radiat Oncol Biol Phys. 2010;77:1403–10.
90. Cher LM, et al. Correlation of hypoxic cell fraction and angiogenesis with glucose metabolic rate in gliomas using 18F-fluoromisonidazole, 18F-FDG PET, and immunohistochemical studies. J Nucl Med. 2006;47:410–8.
91. Lee ST, Scott AM. Hypoxia positron emission tomography imaging with 18f-fluoromisonidazole. Semin Nucl Med. 2007;37:451–61.
92. Yang DJ, et al. Development of F-18-labeled fluoroerythronitroimidazole as a PET agent for imaging tumor hypoxia. Radiology. 1995;194:795–800.
93. Grönroos T, et al. Pharmacokinetics of [18F] FETNIM: a potential marker for PET. J Nucl Med. 2001;42:1397–404.
94. Grönroos T, et al. Comparison of the biodistribution of two hypoxia markers [18F]FETNIM and [18F] FMISO in an experimental mammary carcinoma. Eur J Nucl Med Mol Imaging. 2004;31:513–20.
95. Lehtiö K, et al. Imaging of blood flow and hypoxia in head and neck cancer: initial evaluation with [(15) O]H(2)O and [(18)F]fluoroerythronitroimidazole PET. J Nucl Med. 2001;42:1643–52.
96. Lehtiö K, et al. Quantifying tumour hypoxia with fluorine-18 fluoroerythronitroimidazole ([18F] FETNIM) and PET using the tumour to plasma ratio. Eur J Nucl Med Mol Imaging. 2003;30:101–8.
97. Lehtiö K, et al. Imaging perfusion and hypoxia with PET to predict radiotherapy response in head-and-neck cancer. Int J Radiat Oncol Biol Phys. 2004;59:971–82.
98. Li L, et al. Comparison of 18F-fluoroerythronitro imidazole and 18F-fluorodeoxyglucose positron emission tomography and prognostic value in locally advanced non-small-cell lung cancer. Clin Lung Cancer. 2010;11:335–40.
99. Vercellino L, et al. Hypoxia imaging of uterine cervix carcinoma with (18)F-FETNIM PET/CT. Clin Nucl Med. 2012;37:1065–8.
100. Reischl G, et al. Imaging of tumor hypoxia with [124I]IAZA in comparison with [18F]FMISO and [18F]FAZA – first small animal PET results. J Pharm Pharm Sci. 2007;10:203–11.
101. Kumar P, et al. Fluoroazomycin arabinoside (FAZA): synthesis, 2H and 3H-labelling and preliminary biological evaluation of a novel 2-nitroimidazole marker of tissue hypoxia. J Label Compd Radiopharm. 1999;42:3–16.
102. Kumar P, et al. Microwave-assisted (radio) halogenation of nitroimidazole-based hypoxia markers. Appl Radiat Isot. 2002;57:697–703.
103. Piert M, et al. Hypoxia-specific tumor imaging with 18F-fluoroazomycin arabinoside. J Nucl Med. 2005;46:106–13.
104. SorgerD,etal.[18F]Fluoroazomycinarabinofuranoside (18FAZA) and [18F]fluoromisonidazole (18FMISO): a comparative study of their selective uptake in hypoxic cells and PET imaging in experimental rat tumors. Nucl Med Biol. 2003;30:317–26.
105. Busk M, et al. Imaging hypoxia in xenografted and murine tumors with 18F-fluoroazomycin arabinoside: a comparative study involving microPET, autoradiography, PO2-polarography, and fluorescence microscopy. Int J Radiat Oncol Biol Phys. 2008;70:1202–12.
106. Tran LB, et al. Hypoxia imaging with the nitroimidazole 18F-FAZA PET tracer: a comparison with

OxyLite, EPR oximetry and 19F-MRI relaxometry. Radiother Oncol. 2012;105:29–35.
107. Beck R, et al. Pretreatment 18F-FAZA PET predicts success of hypoxia-directed radiochemotherapy using tirapazamine. J Nucl Med. 2007;48: 973–80.
108. Busk M, et al. PET hypoxia imaging with FAZA: reproducibility at baseline and during fractionated radiotherapy in tumour-bearing mice. Eur J Nucl Med Mol Imaging. 2013;40:186–97.
109. Havelund BM, et al. Tumour hypoxia imaging with 18F-fluoroazomycinarabinofuranoside PET/CT in patients with locally advanced rectal cancer. Nucl Med Commun. 2013;34:155–61.
110. Souvatzoglou M, et al. Tumour hypoxia imaging with [18F]FAZA PET in head and neck cancer patients: a pilot study. Eur J Nucl Med Mol Imaging. 2007;34:1566–75.
111. Postema EJ, et al. Initial results of hypoxia imaging using 1-alpha-D: -(5-deoxy-5-[18F]-fluoroarabinofuranosyl)-2-nitroimidazole (18F-FAZA). Eur J Nucl Med Mol Imaging. 2009;36:1565–73.
112. Mortensen LS, et al. FAZA PET/CT hypoxia imaging in patients with squamous cell carcinoma of the head and neck treated with radiotherapy: results from the DAHANCA 24 trial. Radiother Oncol. 2012;105:14–20.
113. Tewson TJ. Synthesis of [18F]fluoroetanidazole: a potential new tracer for imaging hypoxia. Nucl Med Biol. 1997;24:755–60.
114. Barthel H, et al. In vivo evaluation of [18F]fluoroetanidazole as a new marker for imaging tumour hypoxia with positron emission tomography. Br J Cancer. 2004;90:2232–42.
115. Rasey JS, et al. Characterization of [18F]fluoroetanidazole, a new radiopharmaceutical for detecting tumor hypoxia. J Nucl Med. 1999;40:1072–9.
116. Evans SM, et al. Noninvasive detection of tumor hypoxia using the 2-nitroimidazole [18F]EF1. J Nucl Med. 2000;41:327–36.
117. Christian N, et al. Determination of tumour hypoxia with the PET tracer [18F]EF3: improvement of the tumour-to-background ratio in a mouse tumour model. Eur J Nucl Med Mol Imaging. 2007;34:1348–54.
118. Ziemer LS, et al. Noninvasive imaging of tumor hypoxia in rats using the 2-nitroimidazole 18F-EF5. Eur J Nucl Med Mol Imaging. 2003;30:259–66.
119. Koch CJ, et al. Pharmacokinetics of EF5 [2-(2-nitro-1-H-imidazol-1-yl)-N-(2,2,3,3,3-pentafluoropropyl) acetamide] in human patients: implications for hypoxia measurements in vivo by 2-nitroimidazoles. Cancer Chemother Pharmacol. 2001;48:177–87.
120. Dolbier Jr WR, et al. [18F]-EF5, a marker for PET detection of hypoxia: synthesis of precursor and a new fluorination procedure. Appl Radiat Isot. 2001;54:73–80.
121. Komar G, et al. 18F-EF5: a new PET tracer for imaging hypoxia in head and neck cancer. J Nucl Med. 2008;49:1944–51.
122. Evans SM, et al. Comparative measurements of hypoxia in human brain tumors using needle electrodes and EF5 binding. Cancer Res. 2004;64:1886–92.
123. Evans SM, et al. EF5 binding and clinical outcome in human soft tissue sarcomas. Int J Radiat Oncol Biol Phys. 2006;64:922–7.
124. Wood KA, et al. [(64)Cu]diacetyl-bis(N(4)-methylthiosemicarbazone) – a radiotracer for tumor hypoxia. Nucl Med Biol. 2008;35:393–400.
125. Vavere AL, Lewis JS. Cu-ATSM: a radiopharmaceutical for the PET imaging of hypoxia. Dalton Trans. 2007; (43):4893–4902
126. Lewis JS, et al. Evaluation of 64Cu-ATSM in vitro and in vivo in a hypoxic tumor model. J Nucl Med. 1999;40:177–83.
127. Dearling JL, et al. Copper bis(thiosemicarbazone) complexes as hypoxia imaging agents: structure-activity relationships. J Biol Inorg Chem. 2002;7:249–59.
128. Lewis JS, et al. Tumor uptake of copper-diacetyl-bis(N(4)-methylthiosemicarbazone): effect of changes in tissue oxygenation. J Nucl Med. 2001;42:655–61.
129. Fujibayashi Y, et al. Comparative studies of Cu-64-ATSM and C-11-acetate in an acute myocardial infarction model: ex vivo imaging of hypoxia in rats. Nucl Med Biol. 1999;26:117–21.
130. Yuan H, et al. Intertumoral differences in hypoxia selectivity of the PET imaging agent 64Cu(II)-diacetyl-bis(N4-methylthiosemicarbazone). J Nucl Med. 2006;47:989–98.
131. Burgman P, et al. Cell line-dependent differences in uptake and retention of the hypoxia-selective nuclear imaging agent Cu-ATSM. Nucl Med Biol. 2005;32:623–30.
132. Matsumoto K, et al. The influence of tumor oxygenation on hypoxia imaging in murine squamous cell carcinoma using [64Cu]Cu-ATSM or [18F]fluoromisonidazole positron emission tomography. Int J Oncol. 2007;30:873–81.
133. Bowen SR, et al. Characterization of positron emission tomography hypoxia tracer uptake and tissue oxygenation via electrochemical modeling. Nucl Med Biol. 2011;38:771–80.
134. Katano K, et al. The copper export pump ATP7B modulates the cellular pharmacology of carboplatin in ovarian carcinoma cells. Mol Pharmacol. 2003;64:466–73.
135. Grigsby PW, et al. Comparison of molecular markers of hypoxia and imaging with (60)Cu-ATSM in cancer of the uterine cervix. Mol Imaging Biol. 2007;9:278–83.
136. Dehdashti F, et al. Assessing tumor hypoxia in cervical cancer by PET with 60Cu-labeled diacetyl-bis(N4-methylthiosemicarbazone). J Nucl Med. 2008;49:201–5.
137. Dehdashti F, et al. In vivo assessment of tumor hypoxia in lung cancer with 60Cu-ATSM. Eur J Nucl Med Mol Imaging. 2003;30:844–50.
138. Dietz DW, et al. Tumor hypoxia detected by positron emission tomography with 60Cu-ATSM as a

predictor of response and survival in patients undergoing neoadjuvant chemoradiotherapy for rectal carcinoma: a pilot study. Dis Colon Rectum. 2008;51:1641–8.
139. Chao KS, et al. A novel approach to overcome hypoxic tumor resistance: Cu-ATSM-guided intensity-modulated radiation therapy. Int J Radiat Oncol Biol Phys. 2001;49:1171–82.
140. Lewis JS, et al. An imaging comparison of 64Cu-ATSM and 60Cu-ATSM in cancer of the uterine cervix. J Nucl Med. 2008;49:1177–82.
141. Pastorekova S, et al. Tumor-associated carbonic anhydrases and their clinical significance. Adv Clin Chem. 2006;42:167–216.
142. Wykoff CC, et al. Hypoxia-inducible expression of tumor-associated carbonic anhydrases. Cancer Res. 2000;60:7075–83.
143. Hoeben BA, et al. PET of hypoxia with 89Zr-labeled cG250-F(ab′)2 in head and neck tumors. J Nucl Med. 2010;51:1076–83.
144. Liao SY, et al. Identification of the MN/CA9 protein as a reliable diagnostic biomarker of clear cell carcinoma of the kidney. Cancer Res. 1997;57:2827–31.
145. Murakami Y, et al. MN/CA9 gene expression as a potential biomarker in renal cell carcinoma. BJU Int. 1999;83:743–7.
146. Uemura H, et al. MN/CA IX/G250 as a potential target for immunotherapy of renal cell carcinomas. Br J Cancer. 1999;81:741–6.
147. Lawrentschuk N, et al. Investigation of hypoxia and carbonic anhydrase IX expression in a renal cell carcinoma xenograft model with oxygen tension measurements and (1)(2)(4)I-cG250 PET/CT. Urol Oncol. 2011;29:411–20.
148. Folkman J. Angiogenesis. Annu Rev Med. 2006;57:1–18.
149. Rey S, Semenza GL. Hypoxia-inducible factor-1-dependent mechanisms of vascularization and vascular remodelling. Cardiovasc Res. 2010;86:236–42.
150. Cowden Dahl KD, et al. Hypoxia-inducible factor regulates alphavbeta3 integrin cell surface expression. Mol Biol Cell. 2005;16:1901–12.
151. Langen KJ, Eschmann SM. Correlative imaging of hypoxia and angiogenesis in oncology. J Nucl Med. 2008;49:515–6.
152. Picchio M, et al. Intratumoral spatial distribution of hypoxia and angiogenesis assessed by 18F-FAZA and 125I-Gluco-RGD autoradiography. J Nucl Med. 2008;49:597–605.
153. Brown JM, Wilson WR. Exploiting tumour hypoxia in cancer treatment. Nat Rev Cancer. 2004;4:437–47.
154. Ling CC, et al. Towards multidimensional radiotherapy (MD-CRT): biological imaging and biological conformality. Int J Radiat Oncol Biol Phys. 2000;47:551–60.
155. Bentzen SM, Gregoire V. Molecular imaging-based dose painting: a novel paradigm for radiation therapy prescription. Semin Radiat Oncol. 2011;21:101–10.
156. Busk M, et al. Resolution in PET hypoxia imaging: voxel size matters. Acta Oncol. 2008;47:1201–10.